Modelling the Movement of Superparamagnetic Beads Engulfed in Endothelial Cells

by

Daniel Pasut

A Thesis Submitted in Partial Fulfillment
of the Requirements for the Degree of
Master of Science
in the
Faculty of Science
Modelling and Computational Science

University of Ontario Institute of Technology

April 2018

Abstract

Modelling the Movement of Superparamagnetic Beads Engulfed in Endothelial Cells

Daniel Pasut
Faculty of Science (Modelling and Computational Science)
University of Ontario Institute of Technology
2018

Colonization of porous scaffolds with cells is of increasing importance for various tissue engineering applications. Controlled placement of human umbilical vein endothelial cells (HUVECs) within a micro-porous, poly-caprolactone scaffold is facilitated with superparamagnetic beads introduced to the cells by phagocytosis. It is shown that the dominant motion of the affected cells is determined by the viscous drag of the medium and the amount of coupling with an externally imposed magnetic field. An efficient numerical scheme to compute the trajectories of the cells is presented as the first step in the optimal placement of a large collections of cells with varying numbers of embedded beads.

Contents

List of Tables

List of Figures

CHAPTER 1

Introduction

The controlled growth of a tissue culture within an external environment is one of a number of approaching milestones in the field of bio-medicine. This controlled growth is typically initiated by seeding cells onto an artificial extracellular matrix, or a scaffold, where the cells can be colonized. The term *seeding* refers to the process whereby the cells are introduced and adhered to a scaffold and typically does not include the trajectories of the cells from their initial position to their ultimate destination within the scaffold. The resulting seeded tissue can be used in a variety of applications, including tissue-engineered vascular grafts and wound repair [1].

In order to grow tissue for medical applications, it must be completed as quickly as possible. In this work, we focus not on the seeding of the cells, but on the trajectories of the cells and how they can be influenced by an applied magnetic field. Magnetic force techniques are useful for directing cells that have a noticeable magnetic moment. For example, red blood cells with their high iron content, are naturally magnetic. Other cells without this property require the inclusion of magnetic material to enhance the magnetic effect. The model presented uses magnetic particles

and an applied magnetic field to control the movement of the cells. With a better understanding of the movement of the cells before they are captured by the scaffold and the ability to influence their movement, the controlled growth of tissue can be improved.

Current Exploration in the Field

Examining the behaviour of superparamagnetic beads engulfed by cells for the purpose of tissue engineering is seldom studied. There is a significant amount of research into the superparamagnetic beads themselves, and the use of these beads, or similar beads in cells for cell separation and tracking.

Properties of Superparamagnetic Beads

The properties and behaviour of magnetic particles has been studied for a number of years; often, in the case of nano-/micro-sized magnetic particles, they have been assumed to experience a force when inside a magnetic field. Shevkoplyas et al.[2] examined a more detailed way of determining the force experienced by these beads. In their derivation, the bead is treated as an ideal magnetic dipole with the magnetic moment equal to the effective moment of the bead. This allows for a residual magnetization of the bead in the absence of an applied magnetic field to be calculated. In principle, determining the base magnetization would require tests to be run prior to the use of the beads, and could be used to refine the trajectory.

While Shekoplyas et al. use a permanent magnet or electromagnet to create a spatially varying magnetic field, which leads to a spatially varying magnetic force, Fallesen et al. [3] show it is possible to construct an electromagnet that applies a spatially uniform force to superparamagnetic beads. The field generated by the magnet will determine the force felt by the beads.

Cell Seeding/Tracking Using Magnetic Particles

When using magnetic fields for the separation of cells, there are two main techniques. Šafařik et al. [4] examines both of these methods. For cells with sufficient magnetic moment, such as red blood cells, no modifications to the cells are necessary, and the presence of a sufficiently strong magnetic field will allow for the cells to be separated from the medium. For cells without a sufficiently strong magnetic moment, it is necessary to load the cells with magnetic particles. The magnetic particles used can range in size from nanometers to micrometers in diameter depending upon the manufacturing technique and the target cell.

There are various methods used in the construction of tissue-engineered vascular grafts (TEVG) and other engineered tissue. Methods include construction from cell sheets, and seeding cells onto scaffolds (biodegradable or decellularized). There are also methods that use biological glue or sealant with these techniques. Cell seeding has been proven to be a critical component in the construction of TEVGs, regardless of the cell type. In a review by Villalona et al. [1], various recent cell seeding techniques are examined and compared. Passive seeding, the most widely used method, uses gravity to seed the cells. It is the least efficient method, being time consuming, and yielding an efficiency of $10-25\%$[1]. A natural extension of this method is to use external magnets to aid in the seeding of cells. Exposing the cells to magnetic particles, allowing them to be engulfed, and then using an external magnet to pull the cells towards the scaffold increases the efficiency of seeding to over 90%. This increased efficiency for seeding allows for less expensive and faster graft production, a critical factor in clinical applications. This dissertation enhances this method by exploring the capability to control the capture location of the cells.

The study by Shimizu et al. [5] examines this magnetic seeding technique for

[1]Percent cell-seeding efficiency $= (1 - (\text{number of unattached cells}/\text{number of seeded cells})) \times 100$.

tissue engineering. Using magnetic nanoparticles that are loaded into the cells, a permanent magnet is placed below the scaffold, and the cells are pulled down into the scaffold. With a magnetic field present, it is found that the efficiency of seeding is over 70%, while the efficiency of the passive seeding method (just gravity) ranges from less than 5% to 20%.

Similar studies have been conducted by Dobson [6] where the beads are not engulfed by the cells, but adhered to the exterior of the cell membrane. In this study, the use of the beads hasa dual purpose; to move the cells while in the presence of a magnetic field with a strong gradient, and changing the behaviour of the cells by manipulating ion channels or surface receptors while in the presence of a magnetic field.

In a review by Corchero et al. [7], various applications of magnetic particles *in vivo* and *in vitro* are examined. It is found that the ability to control the position of particles using a magnetic field in a given media is important to induce their accumulation or separation from similar structures. For treatment of cancer cells, once the particles have accumulated in desired locations, they can be used to initiate cell death by localized heating using an alternating magnetic field.

The size and manufacturing method of the magnetic particle influence the type of magnet the particle is. Using a measure of the magnetophoretic mobility (MM)[2], the response to an applied magnetic field for diamagnetic, paramagnetic and superparamagnetic microparticles are compared by Jin et al. [8]. For paramagnetic and diamagnetic materials, the microparticle MM is independent of the applied field, while for superparamagnetic particles, the MM decreases for an increased field. The findings are independent of the cell the particles are loaded into because the magnetic susceptibility[3] of the cell can be ignored due to the overwhelming

[2]The magnetophoretic mobility is defined as the characteristic property of a magnetic particle that causes it to move in a nonuniform magnetic field.

[3]The magnetic susceptibility is a dimensionless constant that indicates the degree of magnetization of a material in response to an applied magnetic field.

susceptibility of the magnetic beads in contrast to the cell.

Recently, work by Xu et al. [9] examines magnetic particles with varying magnetization and sizes. These factors can significantly affect magnetic cell separation and the movement of the cells. Using commercially available instruments (SQUID, vibrating magnetometer, and Coulter counters), three different particle properties are studied. Using these instruments, the particles were characterized and their MM was determined. With the assumption that the magnetization of the particle is directly proportional to the magnetic field, the velocity due to the magnetic field is easily obtained.

To justify in part the modelling approach used in this work, Table 1.1 summarizes a selection of the setup methods that have been explored.

Simulating Scaffolds

Although not the focus of this work, the natural extension of modelling the properties and movement of cells loaded with magnetic particles, is to model the capturing of these cells by a scaffold. This is important for understanding wound repair, pathology, and understanding the relationship between cells, the extracellular matrix/scaffold, and cell migration. A review in 2005 by Semple et al. [10] discusses key areas of computational systems for modern tissue engineering. This review discusses using models that are made to simulate the movement of cells into a matrix and the capturing of the cells. Simulations have been done using Autodesk Maya[4] to render the matrix while other work treats the capturing and motion within the scaffold as a Markov process.

More recently, Robu et al. [11] do not concern themselves with trajectories of cells, and instead use a Metropolis Monte Carlo method to simulate the seeding

[4]Autodesk Maya is a computer graphics application used to create 3-D animations (www.autodesk.com/maya)

Work	Year	Technique	Notes
Šafařik et al. [4]	1999	Magnetic Isolation	Magnetic and superparamagnetic particles, size range from $50 - 200$ nm to $\gtrsim 1\,\mu$m.
Shimizu et al. [5]	2006	Magnetic	Magnetic nanoparticles 10 nm in diameter are used to compare the affects various commercially available 3D scaffolds have on cell seeding.
Dobson [6]	2008	Magnetic Isolation	Superparamagnetic particles ~ 30 nm in size used for isolation and to explore cellular mechanics.
Jin et al. [8]	2008	Magnetic	Compares cell velocities with various magnetic particle sizes to cause varying magnetic susceptibilities of the cells. Mean magnetic particle size of $6.7\,\mu$m.
Corchero et al. [7]	2009	Magnetic	Magnetic nanoparticles $10 - 100$ nm in diameter. Use of cobalt and nickel based particles is not advised due to toxicity.
Villalona et al. [1]	2010	Review	Details a number of techniques including passive, dynamic (rotation, vacuum), and magnetic methods to seed cells, as well as hybrid methods that combine seeding and scaffold generation.
Xu et al. [9]	2012	Magnetic	Various magnetic microparticles compared, ranging from $\sim 2 - 5\,\mu$m. Particle velocity was tracked using cell tracking velocimetry.

Table 1.1: Brief summary of seeding techniques in the literature.

of cells directly into a three dimensional scaffold. This study examines adhesion of the cells to the scaffold and the use of chemotaxis, a morphogenetic mechanism where a cell moves along a concentration gradient, to direct cell motion. With the addition of chemoattractants into the scaffold, it is suggested that cell seeding can be enhanced.

A basic understanding of magnetism is beneficial to differentiate between the properties of ferromagnetic, diamagnetic, and paramagnetic materials. In Chapter 2 of this dissertation, the types of magnetic materials are explored, and their individual advantages/disadvantages are examined. In Chapter 3, the experimental process is described, whereby the magnetic beads are loaded into cells and seeded within a scaffold. Modelling this experimental process requires having a model for the motion of the cells within a magnetic field which must be computed numerically and is where the thrust of this thesis lies. Towards this end, a process is described in Chapter 4 to achieve an accurate representation of the magnetic field in an efficient manner. With the magnetic field computed, the equation of motion is solved and the trajectory of cells are examined for various conditions in Chapter 5. A brief conclusion and an examination of future work is detailed in Chapter 6.

Finally, we close with a brief word concerning notation. In the remainder of this dissertation, a vector field, say $\mathbf{A} : \mathbb{R}^3 \to \mathbb{R}^3$, will be denoted in boldface, so that $\mathbf{A} = (A_1, A_2, A_3)$. Its length $A = \|\mathbf{A}\|$ will denote the Euclidian length $\|\mathbf{A}\| = (A_1^2 + A_2^2 + A_3^2)^{1/2}$. Unit vectors are denoted as $\{\mathbf{e}_x, \mathbf{e}_y, \mathbf{e}_z\}$ in Cartesian coordinates and when appropriate, $\{\mathbf{e}_r, \mathbf{e}_\theta, \mathbf{e}_z\}$ in cylindrical coordinates.

CHAPTER 2

A Primer on Magnetism

A coherent movement of electrons in a conductive material leads to the generation of a magnetic field, however, thermal fluctuation of electrons do not. In practice, electric currents can be used to generate a magnetic field by passing current through a conductive material such as a wire. For an idealized wire of zero diameter carrying a current of I along the z-axis in cylindrical coordinates (r, θ, z), the magnetic field $\mathbf{B} : \mathbb{R}^3 \setminus \{\mathbf{0}\} \to \mathbb{R}^3$ satisfies

$$\nabla \times \mathbf{B} = \mu_0 \mathrm{I} \mathbf{e}_z \delta(r), \tag{2.1}$$

where μ_0 a proportionality constant and $\delta(r)$ denotes a Dirac delta function[12–14] with a solution of

$$\mathbf{B}(r, \theta, z) = \frac{\mu_0 \mathrm{I}}{2\pi r} \mathbf{e}_\theta. \tag{2.2}$$

Similar reasoning can be made when examining other wire orientations. To generate a stronger magnetic field than a single wire, multiple loops of wire can be used; this type of arrangement is typically called a solenoid. The resulting field

about the solenoid is uniform within the windings and non-uniform outside of the windings. Solenoids are used in a variety of fields, such as security; where solenoids are used as locking mechanisms [15], the automotive industry; where they are used in gearboxes and controls [16], and medicine; where solenoids are used in items ranging from dialysis machines[17] to the growth of tissue in a controlled environment [18].

The non-uniform magnetic field created by the solenoid causes a force to be exerted on magnetic beads when they are within the field. Materials with different magnetic properties react to a magnetic field in different ways.

Para/diamagnetism

Magnetism of materials that are not ferromagnetic can be described by two kinds of magnetism. For a material with all electron spins paired, the magnetic dipoles of the material balance, and the total magnetic moment approaches zero. In the presence of an imposed magnetic field, an induced current flows within the material in such a way as to generate an induced magnetic field that opposes the applied field. Known as Lenz's law, materials with this property are referred to as either paramagnetic or diamagnetic [12, 19, 20].

To differentiate between paramagnetic and diamagnetic materials, one considers the magnetic susceptibility, which is defines as the magnetic moment per unit volume per unit of magnetic field intensity. When the magnetic susceptibility is positive, the material is said to be paramagnetic. In these materials, there must be an odd number of electrons, since the system must have a non-zero spin. In the presence of a magnetic field, the magnetic moments of the material attempt to align. In this case, the induced magnetic field enhances the applied magnetic field. In contrast, diamagnetic materials are described by having a negative magnetic suscepti-

bility.

With both diamagnetic and paramagnetic materials, the generated magnetic field depends on the applied magnetic field. When the applied field is turned off, the material loses its magnetic properties. The magnetic affects of these materials do not depend on their previous exposure to an external field. Collectively, such affects are known as hysteresis. With no hysteretic effects, when a varying magnetic field is applied to either diamagnetic and paramagnetic material, the previous history of the applied magnetic field will not influence the current magnetic field.

The lack of hysteretic effects greatly simplifies the dynamics when attempting to control the movement of an object within a magnetic field. However, paramagnetic and diamagnetic materials are not ideal; the magnetic susceptibility of these materials is small, and require a powerful external magnet to generate a substantial force.

Ferromagnetism

Most materials that are considered *magnetic* are actually ferromagnetic. A material is considered ferromagnetic if, in the absence of a magnetic field, it has a nontrivial magnetic moment. This magnetic moment is dependent on the temperature of the material. Above a particular temperature, called the Curie point [19], the magnetic moment disappears.

At temperatures below the Curie point, the magnetic moment of the material is aligned on a small enough scale. However, the material in question may not have an aligned magnetic moment; the domains may not be aligned. When in the presence of a magnetic field, the material becomes magnetized by two methods. When the magnetic field is weak, domains that align with the magnetic field grow, shifting their boundaries. This process is reversible as long as the magnetic field stays weak

enough. Once the magnetic field increases in strength, the boundary displacements are irreversible. An increasing magnetic field beyond this point causes the domains within the material to rotate [19]. These two processes are described in Figure 2.1.

When the material experiences a magnetic field that is strong enough to cause rotation of domains, it becomes a permanent magnet. The magnetization of these materials is hysteretic, and the domains can only return to their original state by increasing the temperature of the material above the Curie point. A typical hysteresis curve for a ferromagnetic material is shown in Figure 2.2.

Superparamagnetism

Superparamagnetic materials overcome many of the issues found in ferromagnetic, paramagnetic, and diamagnetic materials. Superparamagnetism is ferromagnetism under certain constraints. For a particle to be superparamagnetic, it must be a single domain ferromagnetic particle, or a collection of these single domain particles.

When a ferromagnetic particle is small enough, the energy required to split the particle into multiple magnetic domains is larger than the energy required to remain as a particle with a single magnetic domain. Having a single magnetic domain, these particles behave similarly to paramagnetic particles when exposed to an external magnetic field [21,22]. The lack of any major hysteretic effects allows the movement of superparamagnetic particles to be manipulated in an applied magnetic field repeatedly without the previous magnetization taking effect. Superparamagnetic particles are stronger than paramagnetic particles of similar size due to their collective ferromagnetic nature.

When the nanoscale superparamagnetic particles are fixed in place onto a nonmagnetic core, without the ability to rotate, a homogenization effect occurs due to the various orientations of the particles. The homogenization of the domain orien-

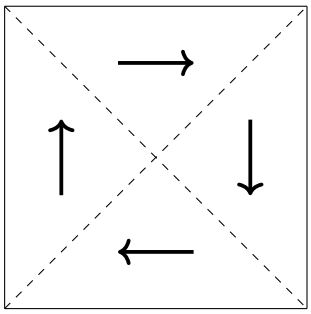

(a) With no applied magnetic field, the material has a net magnetic moment per area of 0.

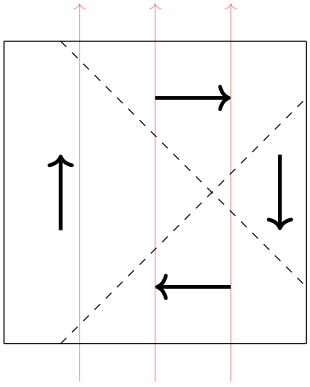

(b) With a weak magnetic field applied, the boundaries of the domains start to shift. With aligned domains having larger areas, the material becomes magnetized.

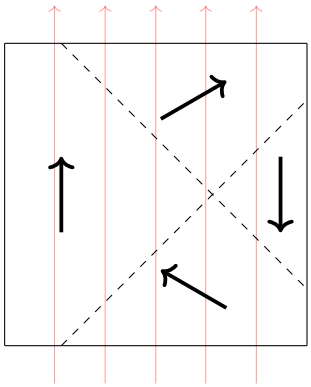

(c) With a strong magnetic field applied, domains begin to rotate. With aligned domains having larger areas, and non-aligned domains rotating, the material becomes permanently magnetized.

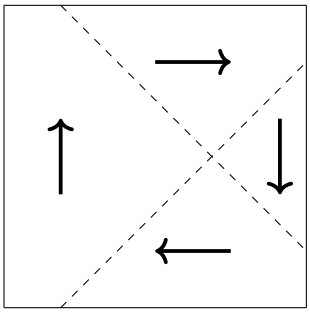

(d) When a material that has experienced a strong applied magnetic field is no in the presence of a magnetic field, it is still magnetized. The boundaries of the domains cannot revert to their original orientation.

Figure 2.1: Domains of a ferromagnetic material with a varying applied magnetic field. The intensity and direction of the applied magnetic field is represented by red arrows.

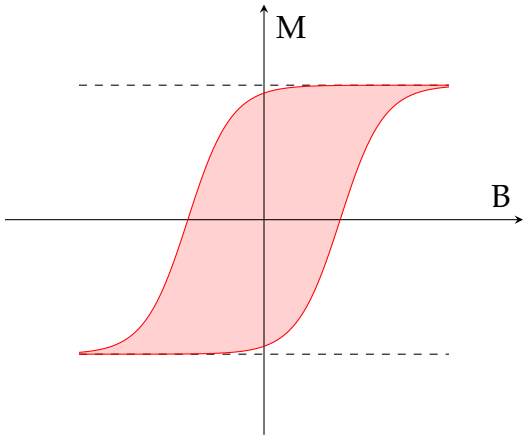

Figure 2.2: Hysteretic magnetization curve for ferromagnetic materials. With an applied magnetic field, the material becomes magnetized. Once the material has experienced a sufficiently strong magnetic field, it cannot become unmagnetized outside of an opposing magnetic field.

tations further reduces the hysteretic effect while increasing the magnet's response to an applied field.

CHAPTER 3

Model

The experiment begins by loading superparamagnetic beads into human umbilical vein endothelial cells (HUVECs). Commercially available superparamagnetic beads can range from an average diameter of $50\,\text{nm}$ to $3.5\,\mu\text{m}$ [23–25]. To utilize the strength of the magnetic field, comparably large superparamagnetic beads, with an average diameter of $3.5\,\mu\text{m}$, are used to control the movement of the cells. These beads are made of a large number of ferromagnetic shavings, fixed in place on the surface of a ceramic core and have a density between $1000\,\text{kg}\,\text{m}^{-3}$ and $1500\,\text{kg}\,\text{m}^{-3}$ [2]. The beads used, MACSiBeads [25], consist of MACSiBead particles coated to anti-biotin antibodies, which encourages their ingestion by the cells.

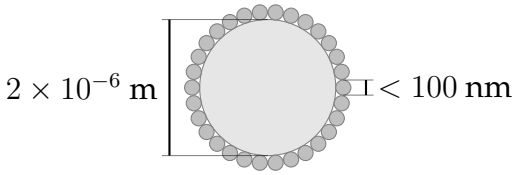

Figure 3.1: A 2-D representation of a superparamagnetic bead, where the exterior of the bead is coated with ferromagnetic particles that are fixed in place.

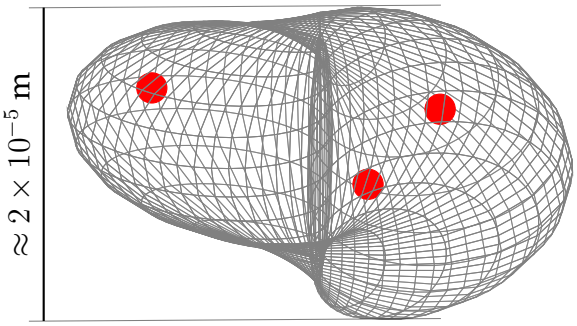

Figure 3.2: A 3-D representation of an HUVEC with engulfed superparamagnetic beads (red). The diameter of the beads is roughly one tenth that of the cell, so multiple beads can be engulfed by a single cell.

The HUVECs are commercially available from Sciencell [26,27]. When the HUVECs come into contact with other particles, they are known to engulf the particles. This is especially useful for the formulation of the model, as the cells retain a uniform shape. The HUVECs have a diameter ranging from $10 - 30\,\mu$m, with a median diameter of $15\,\mu$m, and a density of $\sim 1020\,\mathrm{kg\,m^{-3}}$, compared to water which has a density of $1000\,\mathrm{kg\,m^{-3}}$. To load the superparamagnetic beads into the cells, the cells are stored in an endothelial differentiation medium that contains the antibody-coated superparamagnetic beads.

The superparamagnetic beads are loaded into the cells either by allowing the cells and beads to sit over night in culture, or by a suspension method where the medium is spun for 30 minutes at $37\,°$C. For sufficient loading of the beads in the cells, a bead-to-cell ratio of roughly $20{:}1$ is needed [18]. After the beads have been loaded, an additional step is preformed, where the cells are magnetically sorted to ensure that at least one bead is suspended inside of the cell. The resulting cells have a varying number of beads in each cell (Figure 3.3). This magnetic sorting step is critical for the model, since it guarantees that all cells will experience a force generated by the magnetic field.

After the loading and sorting process is finished, the cells are placed in a tissue

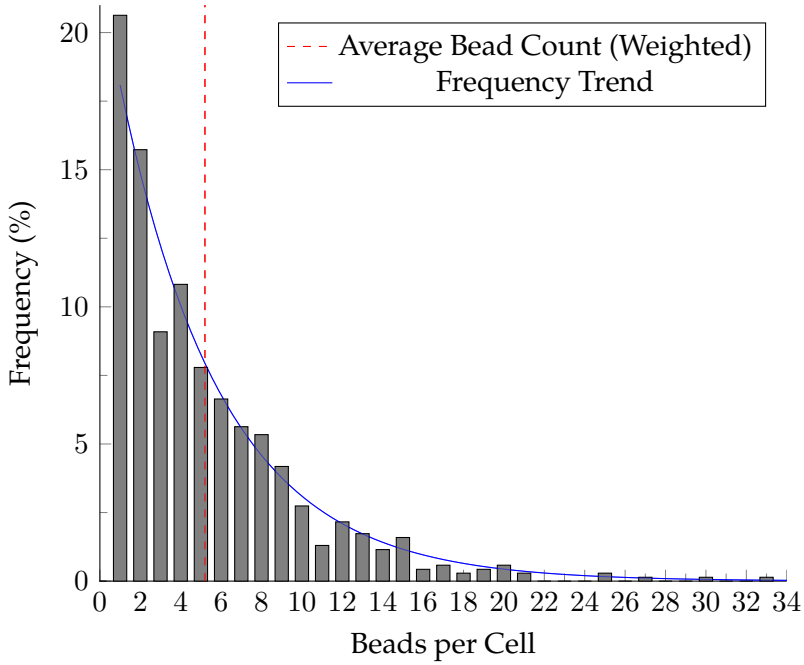

Figure 3.3: Distribution of number of beads found in cells after the magnetic sorting process [18]. Although rare, some cells ingest many beads.

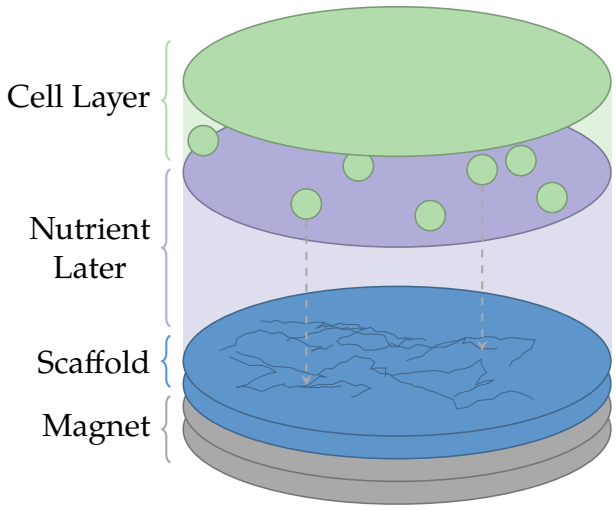

Figure 3.4: Schematic of the cell culture dish. Cells are placed above the nutrient layer, and are pulled down by the applied field towards the scaffold.

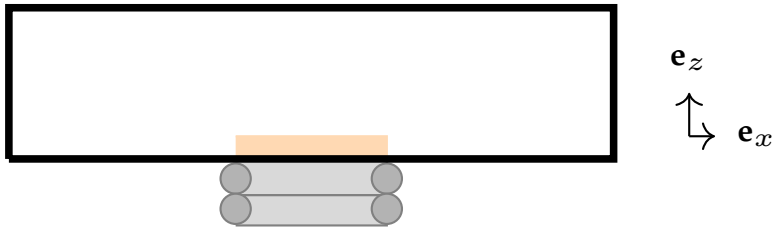

Figure 3.5: Cross sectional representation of the orientation of the tissue culture plate and scaffold (orange) above a solenoid (gray).

culture plate to be colonized on a fibrillar scaffold. The cells are placed onto a nutrient layer, which encourages the growth of the cells with the scaffold at the base of the nutrient layer. A schematic of this can be seen in Figure 3.4. The scaffold has fibers $1-10\,\mu$m in diameter, and has a depth of $\sim 100\,\mu$m. It is cut into small, 18 mm by 18 mm square sheets and adhered along the edges to a tissue culture plate [18].

The tissue culture plate is centered over a solenoid such that the scaffold is directly above centre of the solenoid. With the scaffold directly above the solenoid, the magnetic force will predominantly pull the cells downwards ($-\mathbf{e}_z$ direction) towards the scaffold. The setup is displayed in a simplified, cross sectional representation in Figure 3.5.

To model the scaffold seeding process, the equation of motion for a cell must be determined. The equation of motion can be determined using Newton's second law of motion, $\mathbf{F} = m\mathbf{a}$. In the derivation that follows, the cell membrane is ignored. The cell and all engulfed beads are modeled as a single entity.

Forces

The movement of the cells is controlled by three governing forces. The forces acting in the $\mathbf{e}_z$ direction, gravity and buoyancy, can be combined and described as a single force, $\mathbf{F}_\mathrm{g}$. The force of friction or drag, $\mathbf{F}_\mathrm{f}$, acts in the direction opposite that of the velocity of the object, and the force of magnetism, $\mathbf{F}_\mathrm{m}$, acts in a direction prescribed

Medium			
Parameter	Symbol	Magnitude	Source
Viscosity	μ_w	$10^{-3}\,\mathrm{Pa}\cdot\mathrm{s}$	[28]
Density of water	ρ_w	$1000\,\mathrm{kg\,m^{-3}}$	[28]
Cells			
Parameter	Symbol	Magnitude	Source
Bead density	ρ_b	$1500\,\mathrm{kg\,m^{-3}}$	[29]
Cell density	ρ_c	$1020\,\mathrm{kg\,m^{-3}}$	[29]
Bead diameter	d_b	$2\times10^{-6}\,\mathrm{m}$	[29]
Cell diameter	d_c	$2\times10^{-5}\,\mathrm{m}$	[29]
Magnetism			
Parameter	Symbol	Magnitude	Source
Magnetic susceptibility	χ_{bead}	0.170 ± 0.007	[2]
Permeability of vacuum	μ_0	$4\pi\times10^{-7}\,\mathrm{T\,m\,A^{-1}}$	[2]
Initial magnetization	M_0	$\lesssim 0.17\,\mathrm{A\,m^2\,kg^{-1}}$	[2]

Table 3.1: List of terms and their values used in the formulation of the model. The difference in density between the cells and water is $\Delta\rho = \rho_c - \rho_w = 20\,\mathrm{kg\,m^{-3}}$. The volume of the bead is $V_b = \pi d_b^3/6$, and the volume of the cell can be approximated as $V_c \approx \pi d_c^3/6$.

by the magnetic field, **B**. In combination, the total force can describe the motion of the cells. In the development of the model that follows, a variety of material parameters are required. These have been collected in Table 3.1 for convenience.

To determine the force acting on a cell due to gravity one requires the total mass of a cell of volume V_c containing N_b beads of volume V_b which is given by

$$m_{cell} = (V_c - N_b V_b)\rho_c + N_b V_b \rho_b. \tag{3.1}$$

In addition, the force of buoyancy acts through the centre of the displaced fluid, and since it is assumed that the beads are completely engulfed by the cells, the corresponding mass of the displaced fluid is $m_{fluid} = \rho_w V_c$. Combining these two

gives the gravitational body force of

$$\mathbf{F}_{\mathrm{g}} = (\mathrm{m}_{\text{cell}} - \mathrm{m}_{\text{fluid}})\mathrm{g}(-\mathbf{e}_z) = -\mathrm{g}\left((\rho_{\mathrm{c}} - \rho_{\mathrm{w}})\,\mathrm{V}_{\mathrm{c}} + (\rho_{\mathrm{b}} - \rho_{\mathrm{c}})\,N_{\mathrm{b}}\mathrm{V}_{\mathrm{b}}\right)\mathbf{e}_z. \tag{3.2}$$

As the cell falls through the medium due to gravity, a friction force is experienced in the direction against the motion, commonly referred to as drag. The force of friction is

$$\mathbf{F}_{\mathrm{f}} = -c_{\mathrm{f}}\mu\mathrm{V}_{\mathrm{c}}^{1/3}\dot{\mathbf{X}}, \tag{3.3}$$

where c_{f} is the drag coefficient, μ_{w} is the viscosity of the medium, and $\dot{\mathbf{X}} = \langle \dot{x}, \dot{y}, \dot{z} \rangle$ is the time derivative of the vector $\mathbf{X}$, the position of the cell. When used, $\ddot{\mathbf{X}}$ represents the second time derivative of $\mathbf{X}$. In the case where the cell's shape is approximated by a sphere of radius $\mathrm{d}_{\mathrm{c}}/2$, $c_{\mathrm{f}}\mathrm{V}_{\mathrm{c}}^{1/3} = 3\pi\mathrm{d}_{\mathrm{c}}$ with $\mathrm{V}_{\mathrm{c}} = \pi\mathrm{d}_{\mathrm{c}}^3/6$, recovering the classical drag force of $\mathbf{F}_{\mathrm{f}} = -3\pi\mu_{\mathrm{w}}\mathrm{d}_{\mathrm{c}}\dot{\mathbf{X}}$.

The magnetic force experienced by a body with magnetization $\mathfrak{m}$ and within a magnetic field of $\mathbf{B}$ is given by

$$\mathbf{F}_{\mathrm{m}} = (\mathfrak{m} \cdot \nabla)\mathbf{B} = \left(\mathfrak{m}_x\frac{\partial}{\partial x} + \mathfrak{m}_y\frac{\partial}{\partial y} + \mathfrak{m}_z\frac{\partial}{\partial z}\right)\mathbf{B}. \tag{3.4}$$

For a superparamagnetic material with a specific (per unit mass) magnetization M, due to a permanent component M_0, and a component that varies with an induced magnetic field $\mathbf{B}$,

$$\mathfrak{m} = \rho_{\mathrm{b}}\mathrm{V}_{\mathrm{b}}\mathsf{M} = \rho_{\mathrm{b}}\mathrm{V}_{\mathrm{b}}\left(\mathsf{M}_0 + \frac{\chi_{\text{bead}}}{\rho_{\mathrm{b}}\mu_0}\mathbf{B}\right), \tag{3.5}$$

where μ_0 and χ_{bead} are the magnetic permeability and magnetic susceptibilities respectively. Including the permanent component to the magnetization leads to the expanded form of the magnetic force

$$\mathbf{F}_{\mathrm{m}} = \rho_{\mathrm{b}}\mathrm{V}_{\mathrm{b}}(\mathsf{M}_0 \cdot \nabla)\mathbf{B} + \frac{\mathrm{V}_{\mathrm{b}}\chi_{\text{bead}}}{\mu_0}(\mathbf{B} \cdot \nabla)\mathbf{B}. \tag{3.6}$$

Using Newton's second law of motion, $\mathrm{m}\ddot{\mathbf{X}} = \mathbf{F}_\mathrm{g} + \mathbf{F}_\mathrm{f} + \mathbf{F}_\mathrm{m}$, an equation of motion can be determined,

$$\mathrm{m}\ddot{\mathbf{X}} = -\mathrm{g}\left(\left(\rho_\mathrm{c} - \rho_\mathrm{w}\right)\mathrm{V_c} + \left(\rho_\mathrm{b} - \rho_\mathrm{c}\right)N_\mathrm{b}\mathrm{V_b}\right)\mathbf{e}_z - c_\mathrm{f}\mu\mathrm{V_c}^{1/3}\dot{\mathbf{X}} + (\mathfrak{m}\cdot\nabla)\mathbf{B} \tag{3.7}$$

for $t > 0$ and with given $\mathbf{X}(0), \dot{\mathbf{X}}(0)$.

To determine the magnitude and direction of $\mathbf{B}$, a single loop of a wire with radius a carrying a current of I is examined [12]. Figure 3.6 describes a loop of radius a in the x-y plane parameterized by $s \in [0, 2\pi)$. In this case a vector from the origin to any point on the loop is given by $\mathbf{r}_s = a(\cos s, \sin s, 0)$, and a differential element of the curve is given by $\mathrm{d\mathbf{l}} = a(-\sin s, \cos s, 0)\mathrm{ds}$. The resulting contribution to the magnetic field along the z-axis is given by

$$\mathrm{d}\mathbf{B} = \left.\frac{\mu_0 \mathrm{I}\,\mathrm{d\mathbf{l}} \times (\mathbf{r} - \mathbf{r}_s)}{4\pi\|\mathbf{r} - \mathbf{r}_s\|^3}\right|_{x=y=0} = \left(0, 0, \frac{\mu_0 \mathrm{I}}{4\pi}\frac{a^2\mathrm{ds}}{(a^2+z^2)^{3/2}}\right). \tag{3.8}$$

The resulting magnetic field is then $\mathbf{B} = (0, 0, \mathrm{B}_z)$ with

$$\mathrm{B}_z = \int_{s=0}^{2\pi} \frac{\mu_0 \mathrm{I}}{4\pi}\frac{a^2\mathrm{ds}}{(a^2+z^2)^{3/2}} = \frac{\mu_0 I a^2}{2(a^2+z^2)^{3/2}} \tag{3.9}$$

for a single turn of wire. From this, a characteristic magnetic induction, B_0, can be determined at the position $z = 0$. This gives

$$B_0 = \frac{\mu_0 I a^2}{2a^3} = \frac{\mu_0 I}{2a}. \tag{3.10}$$

For multiple adjacent loops of wire, as in Figure 3.7, carrying the same current I, the accumulated field at $z = 0$ would be

$$\mathrm{B}_z = \sum_{j=1}^{L} \frac{\mu_0 \mathrm{I} a^2}{2}\frac{N_j}{(a^2+z_j^2)^{3/2}}, \tag{3.11}$$

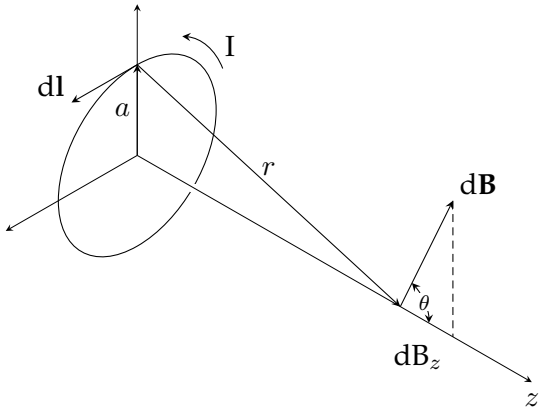

Figure 3.6: The magnetic induction due to a single coil of wire perpendicular to the z-axis. The magnetic induction, d**B**, is produced by a current element I d**l** and measured at a point along the z-axis. The projection of the resulting magnetic induction on the z-axis is dB_z.

where N_j is the number of loops located at axial position z_j for $j = 1, 2, ..., L$. Passing to the limit of a continuum of loops evaluating from $z = -L/2$ to $z = L/2$ and a loop density of N' loops per unit length gives

$$\mathrm{B}_z = \frac{\mu_0 N' a^2}{2} \int_{-L/2}^{+L/2} \frac{\mathrm{d}z}{(a^2 + z^2)^{3/2}} = \frac{\mu_0 N'}{2} \frac{L}{(a^2 + L^2/4)^{1/2}}. \tag{3.12}$$

At either end of the solenoid, which is more relevant to the study of the field outside of the solenoid,

$$\mathrm{B}_z = \mu_0 N' \mathrm{I} \frac{\sin\theta_e}{2}; \tag{3.13}$$

where θ_e is the angle from the relative position along the solenoid $(0, 0, -l/2)$ to $(a, 0, +l/2)$, or $\theta_e = \tan^{-1}(a/l)$ which gives

$$\mathrm{B}_z = \frac{\mu_0 N' \mathrm{I} a}{2(a^2 + l^2)^{1/2}}. \tag{3.14}$$

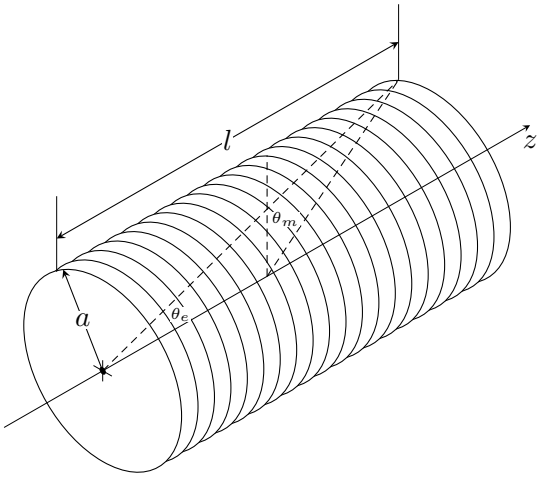

Figure 3.7: Approximation of a short solenoid of length l and radius a aligned along the z-axis using concentric loops of wire, unlike a solenoid which has a single wire with $p > 0$.

Nondimensionalization

In the absence of a magnetic field, cells rapidly reach a terminal velocity of

$$\mathbf{v}_\infty = -\frac{g}{3\pi\mu_\mathrm{w}\mathrm{d_c}}\left(\Delta\rho\mathrm{V_c} + (\rho_\mathrm{b} - \rho_\mathrm{c})N_\mathrm{b}\mathrm{V_b}\right)\mathbf{e}_z = -v_\infty\mathbf{e}_z,$$

so that positive values of $v_\infty = \|\mathbf{v}_\infty\|$ indicate downward motion. Choosing a length and time scale consistent with this speed, $\mathbf{X} = L\tilde{\mathbf{X}}$, $t = L\tilde{t}/v_\infty$, allows one to rewrite (3.7) as

$$\epsilon(N_\mathrm{b})\frac{\mathrm{d}^2}{\mathrm{d}\tilde{t}^2}\tilde{\mathbf{X}} = -\left(\mathbf{e}_z + \frac{\mathrm{d}}{\mathrm{d}\tilde{t}}\tilde{\mathbf{X}}\right) + \Gamma(N_\mathrm{b})\left(\left(\frac{\mathsf{M}_0}{B_0}\cdot\tilde{\nabla}\right)\tilde{\mathbf{B}} + \frac{\chi_\mathrm{bead}}{\rho_\mathrm{b}\mu_0}(\tilde{\mathbf{B}}\cdot\tilde{\nabla})\tilde{\mathbf{B}}\right), \tag{3.15}$$

where

$$\Gamma(N_\mathrm{b}) = \frac{\rho_\mathrm{b}N_\mathrm{b}\mathrm{V_b}B_0^2}{3\pi\mu_\mathrm{w}\mathrm{d_c}v_\infty L} = \frac{\rho_\mathrm{b}B_0^2\mathrm{V_b}}{\Delta\rho g L\mathrm{V_c}}\left(\frac{N_\mathrm{b}}{1 + \dfrac{(\rho_\mathrm{b} - \rho_\mathrm{c})\mathrm{V_b}N_\mathrm{b}}{\Delta\rho\mathrm{V_c}}}\right). \tag{3.16}$$

Choosing a characteristic magnetic induction (3.10) such that $\mathbf{B} = B_0\tilde{\mathbf{B}}$ and

$$\epsilon(N_\mathrm{b}) = \frac{\mathrm{m}_\mathrm{cell} v_\infty}{3\pi\mu_\mathrm{w}\mathrm{d}_\mathrm{c}L} = \epsilon_0(1 + \epsilon_1 N_\mathrm{b} + \epsilon_2 N_\mathrm{b}^2) \tag{3.17}$$

with

$$\epsilon_0 = \left(\frac{\rho_\mathrm{c}\mathrm{V}_\mathrm{c}}{3\pi\mu_\mathrm{w}\mathrm{d}_\mathrm{c}L}\right)^2 \frac{\Delta\rho}{\rho_\mathrm{c}} gL, \quad \epsilon_1 = (\rho_\mathrm{b} - \rho_\mathrm{c})\left(\frac{1}{\Delta\rho} + \frac{1}{\rho_\mathrm{c}}\right)\frac{\mathrm{V}_\mathrm{b}}{\mathrm{V}_\mathrm{c}}, \quad \epsilon_2 = \frac{\rho_\mathrm{c}}{\Delta\rho}\left(\frac{(\rho_\mathrm{b} - \rho_\mathrm{c})\mathrm{V}_\mathrm{b}}{\rho_\mathrm{c}\mathrm{V}_\mathrm{c}}\right)^2,$$

and letting the characteristic length be the approximate depth of the tissue culture plate, $L = 1$ cm, we find that $v_\infty \simeq 4.5 \times 10^{-6}\ \mathrm{m\,s^{-1}}$ when including a single bead, $\epsilon_0 = 9.9 \times 10^{-9}$, $\epsilon_1 = 2.4 \times 10^{-2}$, and $\epsilon_2 = 1.1 \times 10^{-5}$. Figure 3.8 illustrates ϵ as a function of the number of beads within the cell. Although quadratic, for realistic values of $N_\mathrm{b} \lesssim 40$, ϵ can be approximated by a linear function with a slope of $\epsilon_0\epsilon_1 \sim 2.4 \times 10^{-10}$.

The behaviour of $\Gamma(N_\mathrm{b})$ for N_b approaching 0 is determined by expanding

$$\begin{aligned}\Gamma(N_\mathrm{b}) &= \frac{\rho_\mathrm{b} B_0^2 \mathrm{V}_\mathrm{b}}{\Delta\rho g L \mathrm{V}_\mathrm{c}} \left(\frac{N_\mathrm{b}}{1 + \dfrac{(\rho_\mathrm{b} - \rho_\mathrm{c})\mathrm{V}_\mathrm{b} N_\mathrm{b}}{\Delta\rho \mathrm{V}_\mathrm{c}}}\right) \\ &= \frac{\rho_\mathrm{b} B_0^2 \mathrm{V}_\mathrm{b} N_\mathrm{b}}{\Delta\rho g L \mathrm{V}_\mathrm{c}} \left(1 - \epsilon^* N_\mathrm{b} + \mathcal{O}(\epsilon^*)\right) \approx \frac{\rho_\mathrm{b} B_0^2 \mathrm{V}_\mathrm{b}}{\Delta\rho g L \mathrm{V}_\mathrm{c}} N_\mathrm{b} = \Gamma_0(N_\mathrm{b}),\end{aligned} \tag{3.18}$$

where

$$\epsilon^* = \frac{\Delta\rho \mathrm{V}_\mathrm{c}}{(\rho_\mathrm{b} - \rho_\mathrm{c})\mathrm{V}_\mathrm{b}} \ll 1.$$

The limit of $\Gamma(N_\mathrm{b})$ as $N_\mathrm{b} \to \infty$ indicates the behaviour of Γ for a large number of beads, resulting in

$$\Gamma_\infty = \lim_{N_\mathrm{b}\to\infty} \Gamma(N_\mathrm{b}) = \lim_{N_\mathrm{b}\to\infty} \frac{\rho_\mathrm{b} B_0^2 \mathrm{V}_\mathrm{b}}{\Delta\rho g L \mathrm{V}_\mathrm{c}} \left(\frac{N_\mathrm{b}}{1 + \dfrac{(\rho_\mathrm{b} - \rho_\mathrm{c})\mathrm{V}_\mathrm{b} N_\mathrm{b}}{\Delta\rho \mathrm{V}_\mathrm{c}}}\right) = \frac{\rho_\mathrm{b} B_0^2}{(\rho_\mathrm{b} - \rho_\mathrm{c}) g L}. \tag{3.19}$$

A characteristic number of beads, N_b^*, which indicates the approximate number of beads required to switch from the Γ_0 to the Γ_∞ regime is found by setting $\Gamma_0(N_\mathrm{b}^*) = \Gamma_\infty$ so that

$$N_\mathrm{b}^* = \frac{(\rho_\mathrm{b} - \rho_\mathrm{c})\mathrm{V_b}}{\Delta\rho \mathrm{V_c}} \approx 40. \tag{3.20}$$

With less than 40 beads being captured by the cells, as seen in Figure 3.3 which indicates the maximum number of captured cells being 33, the influence of the magnetic induction scales at most linearly with an increasing number of beads, as the value of Γ reaches an asymptote at Γ_∞. This behaviour is observed in Figure 3.9.

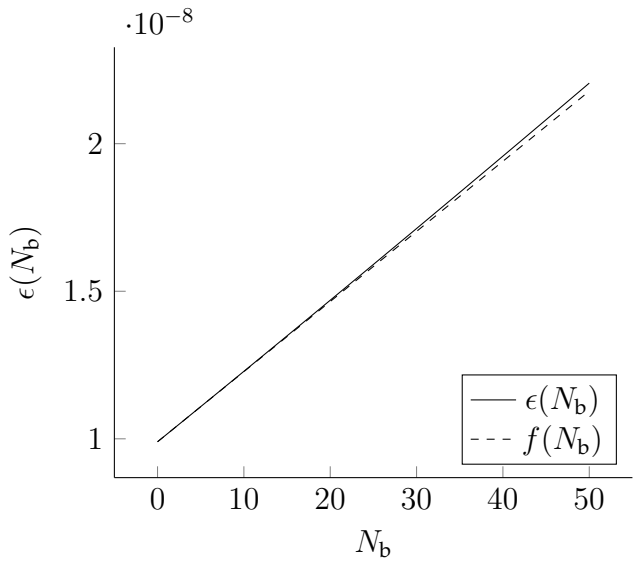

Figure 3.8: Comparison of $\epsilon(N_\mathrm{b})$ with the linear approximation $f(N_\mathrm{b}) = \epsilon_0(1 + \epsilon_1 N_\mathrm{b})$. Roughly 20 beads are required before the linear dependence becomes significant and about 100 beads are needed to observe the quadratic dependence.

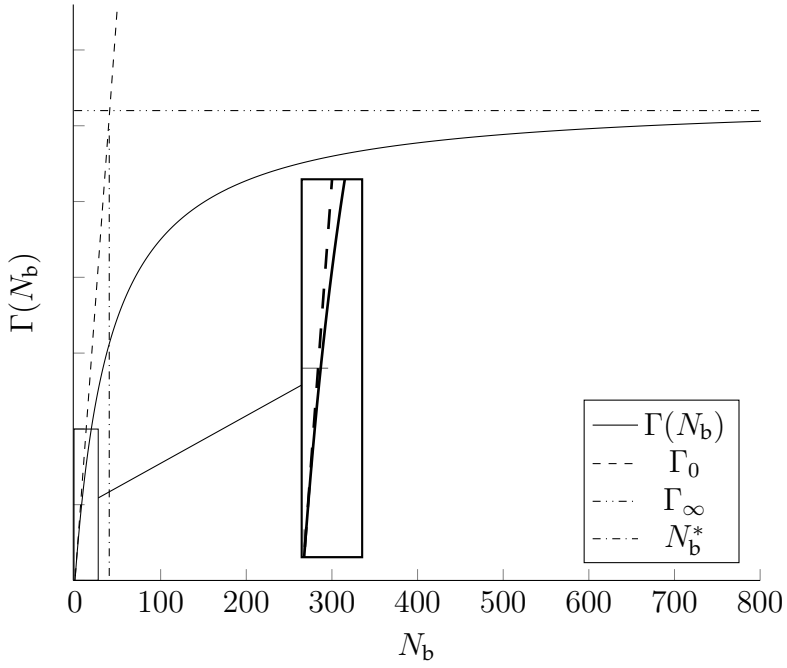

Figure 3.9: The behaviour of $\Gamma(N_\mathrm{b})$ as a function of the number of beads in a cell. When $N_\mathrm{b} < N_\mathrm{b}^*$, Γ is approximately linear with a maximum slope of Γ_0/N_b. When $N_\mathrm{b} > N_\mathrm{b}^*$, $\Gamma(N_\mathrm{b})$ approaches asymptote of Γ_∞.

"Singular" Perturbation Problem

When examining (3.15) with no magnetic present, the equation can be simplified to the equation of motion

$$\epsilon\ddot{z} = -1 - \dot{z}, \qquad z(0) = 1, \dot{z}(0) = v_0 \tag{3.21}$$

where $\dot{z} = \mathbf{e}_z \cdot \frac{\mathrm{d}}{\mathrm{d}\tilde{t}}\tilde{\mathbf{X}}$, $\ddot{z} = \mathbf{e}_z \cdot \frac{\mathrm{d}^2}{\mathrm{d}\tilde{t}^2}\tilde{\mathbf{X}}$, and v_0 is the initial velocity of the cells. With $\epsilon\ddot{z}$ as the highest term, and $\epsilon \ll 1$, problem is considered singular. When looking at the differential equation (3.21) using perturbation theory, the $\mathcal{O}(\epsilon^0)$ component of the solution is only consistent when $v_0 = -1$, yielding the outer solution $z(t) = 1-t$. Solving (3.21) as a nonhomogeneous linear equation with constant coefficients gives a general solution of $z_g(t) = c_0 + c_1\mathrm{e}^{-t/\epsilon}$ and a particular solution of $z_p(t) = -t$,

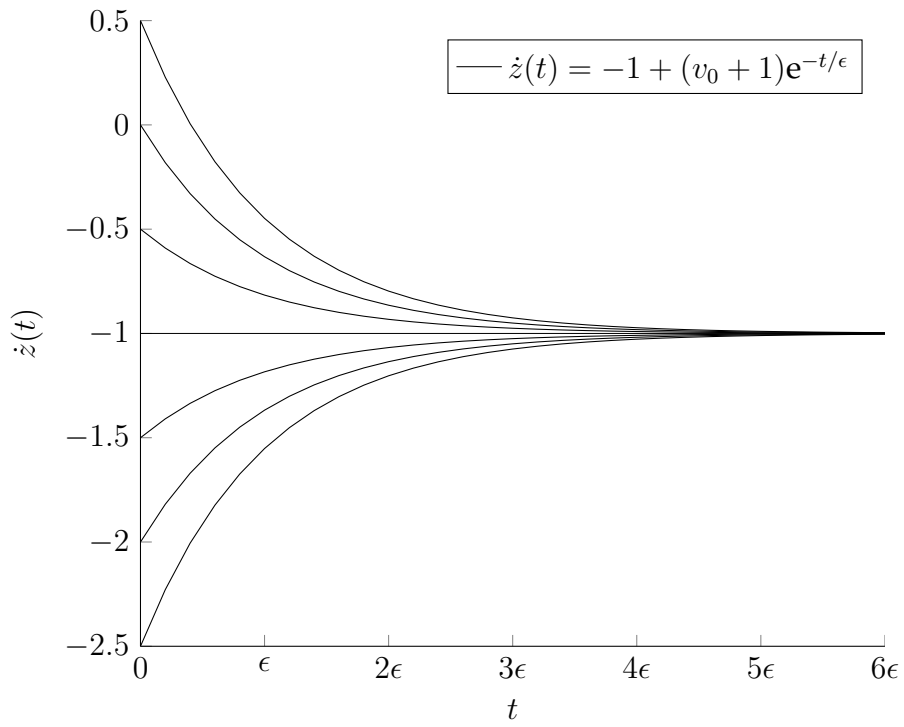

Figure 3.10: Examining multiple v_0 values between -2.5 and 0.5 for $\dot{z}(t)$, an asymptote is reached at $\dot{z}(t) = -1$.

when combined with the initial conditions yields the exact solution

$$z_{\text{exact}}(t) = (1 - t) + \epsilon(v_0 + 1)(1 - \mathrm{e}^{-t/\epsilon}). \tag{3.22}$$

Regardless of the initial velocity, the velocity of the cell reaches terminal velocity, $\dot{z}(t) = -1$, within $t \ll 1$, which satisfies the condition on the approximation $z(t) = 1 - t$. This can be seen in Figure 3.10. In the time it takes for the velocity of the cell to reach terminal velocity, the error between the approximation $z(t)$ and the exact solution $z_{\text{exact}}(t)$ increases. The maximum error is achieved at $\lim_{t\to\infty} z_{\text{exact}}(t) - z(t) = \epsilon(v_0 + 1)$. The boundary layer found in (3.22) is $\mathcal{O}(\epsilon)$, and is observed before the cell reaches terminal velocity. This can be seen in Figure 3.11.

When examining (3.15) in a single dimension *with* the magnetic field present,

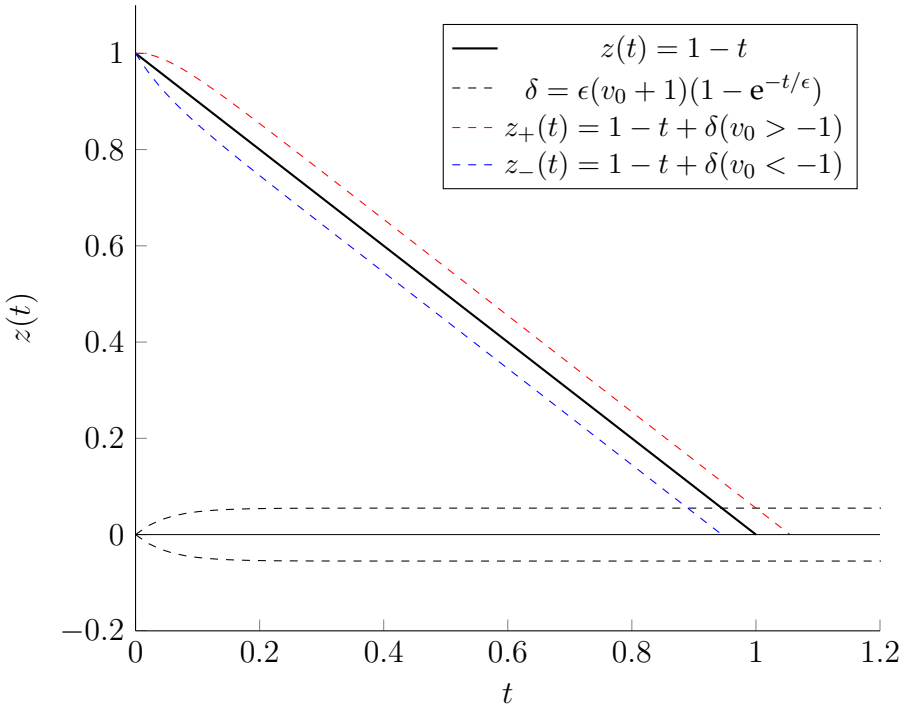

Figure 3.11: With a given initial velocity of the cell v_0, the solution of the differential equation is within δ of the simplified differential equation $z(t) = 1 - t$. When the initial velocity is $v_0 = -1$, $\delta = 0$, giving $z(t)$. However, because $\epsilon \ll 1$, the increased time required for $z(t)$ to reach $z = 0$ is minimal, and can be ignored.

the simplified equation of motion becomes

$$\epsilon\ddot{z} = -1 - \dot{z} + f(z), \qquad z(0) = 1, \dot{z}(0) = v_0, \tag{3.23}$$

where $f(z)$ is the resulting z component from the magnetic force. This equation cannot be easily analyzed as was done with (3.21). However, the properties of the system are consistent, and an outer solution can be found by solving the differential equation

$$\dot{z}(t) = -1 + f(z). \tag{3.24}$$

In the outer solution, the three terms in this equation are $\mathcal{O}(1)$ while $\ddot{z}(t) \in \mathcal{O}(\epsilon)$, and can be ignored for the approximation. Within the boundary layer, the velocity is $\mathcal{O}(\epsilon)$ as before, so to balance (3.24), $f(z) \sim \mathcal{O}(1)$. This is consistent with what is expected, because when the magnetic field is present, the cells reach the base of the cell culture dish ~ 4 times faster, which is $\mathcal{O}(1)$.

The inertial term $\epsilon\frac{\mathrm{d}^2}{\mathrm{d}\tilde{t}^2}\tilde{\mathbf{X}}$, from the equation of motion of a cell (3.15), is $\mathcal{O}(\epsilon)$. This allows an approximate form of (3.15) to be written as

$$\frac{\mathrm{d}}{\mathrm{d}\tilde{t}}\tilde{\mathbf{X}} = -\mathbf{e}_z + \Gamma(N_\mathrm{b})\left(\left(\frac{\mathsf{M}_0}{B_0}\cdot\tilde{\nabla}\right)\tilde{\mathbf{B}} + \frac{\chi_\mathrm{bead}}{\rho_\mathrm{b}\mu_0}(\tilde{\mathbf{B}}\cdot\tilde{\nabla})\tilde{\mathbf{B}}\right), \tag{3.25}$$

with $\Gamma(N_\mathrm{b})$ as in (3.16), and characteristic length and time scales given by $L = 1$ cm and $T = L/v_\infty \approx 37$ minutes. With an efficient computation of the nondimensionalized applied magnetic field, the trajectory of a cell can be determined.

CHAPTER 4

Computation of the Magnetic Force

Determination of the path the cells take when under the influence of a magnetic field is of primary importance. In this modelling effort the external magnetic field that bathes the cells is assumed to be generated by a solenoid located outside of the tissue culture plate.

In the literature, determination of the magnetic field caused by a solenoid is often focused on either the interior of a finite length solenoid, or outside of an infinitely long solenoid [14,30,31]. In addition, the field has also been routinely studied along the axis of a finite length solenoid [12], drastically simplifying its functional form. This chapter describes the numerical solution of the magnetic field of a nonidealized solenoid for any point outside of its wire assembly. The resulting force experienced by any given cell by the superparamagnetic effect acting on the ingested magnetic beads can then be determined.

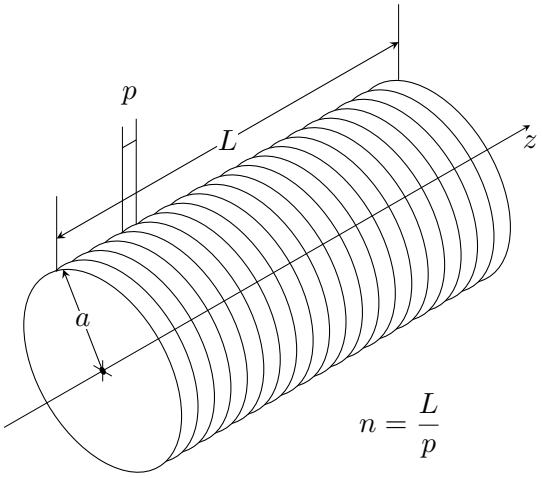

Figure 4.1: Visualization of a uniform single wrapping of wire for the solenoid; p is the pitch of the coils, a is the radius of the coils, n is the number of coils that make the solenoid, and L is the length.

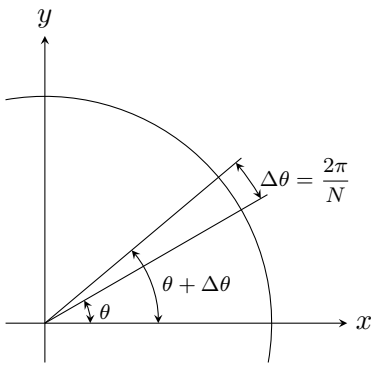

Figure 4.2: Visualization of $\Delta\theta$ on a single coil of the solenoid.

Magnetic Field

Analytically solving for the magnetic field outside of the solenoid is typically achieved by first evaluating the vector potential of the magnetic field, **A**, at a given point and then computing $\mathbf{B} = \nabla \times \mathbf{A}$ [32–34]. The method used here for solving **B** is the first of two methods used by Basu et al. in [32], and involves each coil of the wire being broken up into N segments, computing the contribution of each and then summing over all contributions.

For a segment with curve element $d\mathbf{l}$, the corresponding magnetic induction is

given by

$$\mathrm{d}\mathbf{B} = \frac{\mu_0 \mathrm{I}}{4\pi} \frac{\mathrm{d}\mathbf{l} \times \mathbf{r}}{\|\mathbf{r}\|^3}, \tag{4.1}$$

where $\mathbf{r}$ is the vector from the curve element, dl, to the reference point where the magnetic field is calculated. In the case of a helical wire of radius a and pitch $2\pi b$, the path of the centre of the wire loops is given by

$$\mathbf{l}(t) = \langle a\cos t, a\sin t, bt\rangle. \tag{4.2}$$

The pitch, as seen in Figure 4.1, is described as the displacement in the $\mathbf{e}_z$ direction after a revolution of 2π so that $p = \mathbf{e}_z \cdot (\mathbf{l}(t+2\pi) - \mathbf{l}(t)) = 2\pi b$. The length of the solenoid L, number of coils n, and radius of the coil a can also be seen in Figure 4.1.

As mentioned previously, each turn of the coil is split into N segments, each with a length of

$$\Delta\theta = \frac{2\pi}{N}. \tag{4.3}$$

See Figure 4.2. With the z-axis being set along the length of the solenoid, and with the solenoid having a helical shape described in Eq. (4.2), the m^{th} curve segment is given by

$$\Delta\mathbf{l}_m = \mathbf{l}(\theta_m) - \mathbf{l}(\theta_{m-1}) = a(1-\cos(\Delta\theta))\hat{\mathbf{r}}_m + a\sin(\Delta\theta)\hat{\theta}_m + \frac{p}{N}\mathbf{e}_z, \tag{4.4}$$

where the unit vector from the origin to the position at θ_m is $\hat{\mathbf{r}}_m = \langle\cos\theta_m, \sin\theta_m, 0\rangle$, and with a perpendicular vector $\hat{\theta}_m = \langle -\sin\theta_m, \cos\theta_m, 0\rangle$. A vector from the origin

to the centre of the m^{th} curve element is then

$$\begin{aligned}\mathbf{r}_s(\theta_m) &= \mathbf{l}(\theta_m - \Delta\theta/2) \\ &= \left\langle a\cos\left(\theta_m - \frac{1}{2}\Delta\theta\right), a\sin\left(\theta_m - \frac{1}{2}\Delta\theta\right), \frac{p}{2\pi}\left(\theta_m - \frac{1}{2}\Delta\theta\right)\right\rangle \\ &= a\cos\left(\frac{1}{2}\Delta\theta\right)\hat{\mathbf{r}}_m - a\sin\left(\frac{1}{2}\Delta\theta\right)\hat{\theta}_m + \frac{p}{2N}(2m-1)\mathbf{e}_z. \end{aligned} \tag{4.5}$$

The vector from some reference location $\mathbf{X}_{i,j,k} = \langle x_i, y_j, z_k\rangle$ to the centre of this element is then

$$\mathbf{r}_{i,j,k}(\theta_m) = \mathbf{r}_m = \mathbf{X}_{i,j,k} - \mathbf{r}_s(\theta_m). \tag{4.6}$$

Using Eq. (4.4) – (4.6) in Eq. (4.1), the magnetic field can be calculated for the m^{th} current element. To determine the total magnetic field at reference point $\mathbf{X}$, the contributions from each curve element must be summed so that,

$$\mathbf{B}(x_i, y_j, z_k) \simeq \frac{\mu_0 \mathrm{I}}{4\pi}\sum_{m=1}^{nN}\frac{\Delta\mathbf{l}(\theta_m)\times\mathbf{r}_m}{\|\mathbf{r}_m\|^3}, \qquad \mathbf{r}_m = \mathbf{X}_{i,j,k} - \mathbf{r}_s(\theta_m). \tag{4.7}$$

With this approximate expression for $\mathbf{B}$, we can determine the magnetic field around the solenoid at discrete grid points $\langle x_i, y_j, z_k\rangle$. Looping over all i, j, k produces the resulting magnetic field seen in Figure 4.3. The code written for the generation of Figure 4.3 can be found in Appendix A.

Magnetic Force

As mentioned above in Section 3.1, the magnetic force contains two main components; the magnetic force due to the magnetic field, and the magnetic force due to the initial magnetization. The magnetic force given by Eq. (3.6) is

$$\mathbf{F}_{\mathrm{m}} = \rho_{\mathrm{b}}\mathrm{V}_{\mathrm{b}}(\mathrm{M}_0\cdot\nabla)\mathbf{B} + \frac{\mathrm{V}_{\mathrm{b}}\chi_{\mathrm{bead}}}{\mu_0}(\mathbf{B}\cdot\nabla)\mathbf{B}.$$

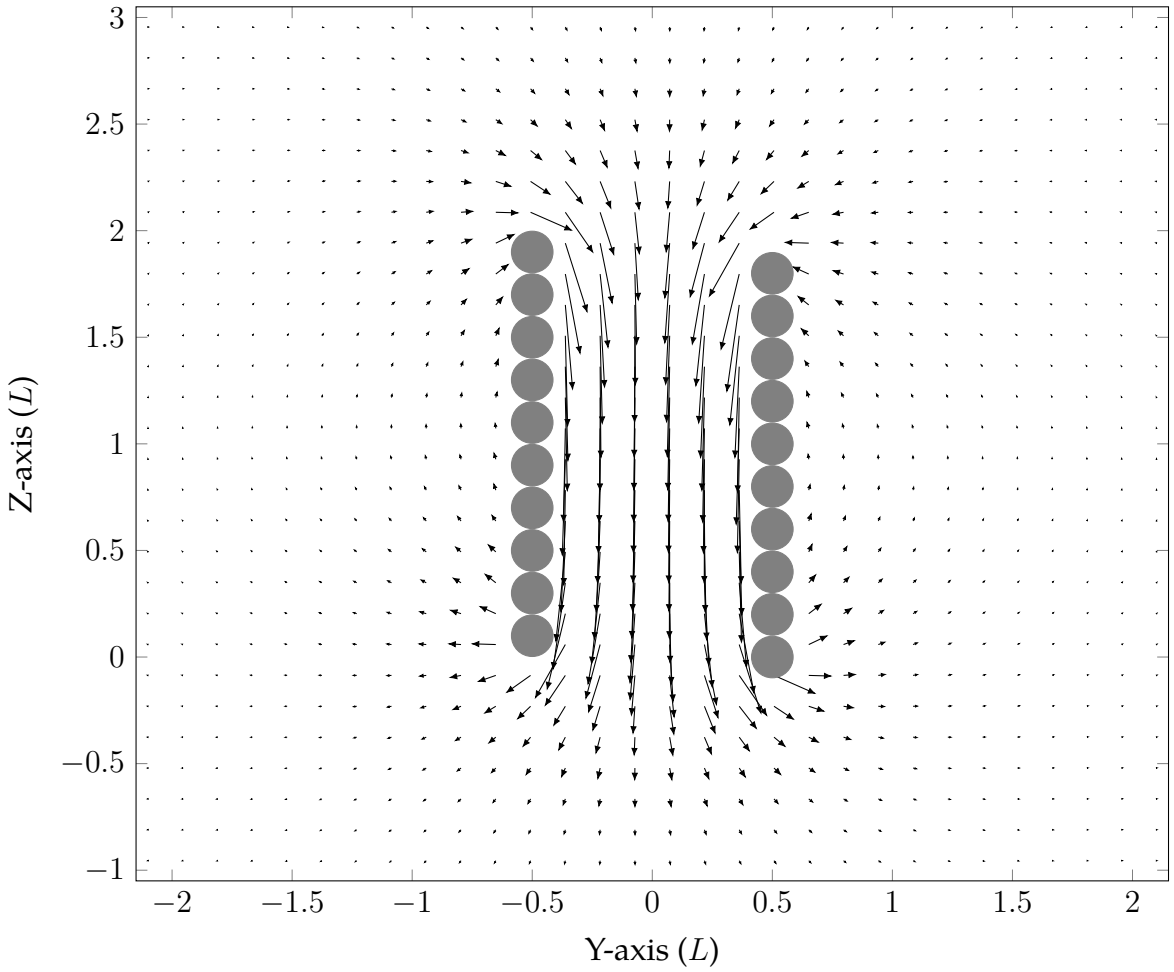

Figure 4.3: Visualization of the magnetic field $\mathbf{B}(0, y, z)$. This visualization has minimal variation at different cross sectional angles. Note that $L = 1$ cm, as in Section 3.2.

Both the magnetic force due to the magnetic field, and the magnetic force due to the initial magnetization can be solved numerically after the magnetic field is solved.

Gradient of the Field

To numerically compute $(\mathbf{B} \cdot \nabla)\mathbf{B}$, the magnetic field must be solved at points surrounding the reference location. In order to avoid excess computations, the magnetic field must be solved at as few locations as possible. The magnetic field must be computed explicitly for positions $\mathbf{X}_{i,j,k} + \epsilon\, \mathbf{e}_y$ and $\mathbf{X}_{i,j,k} + \epsilon\, \mathbf{e}_z$, where ϵ is proportional to the scale of the system. In the $\mathbf{e}_x$ direction, the magnetic field can be solved using properties of the magnetic field. It can be shown that, using the Biot-Savart law (Eq. 4.1), the divergence of the magnetic field is zero [12],

$$\nabla \cdot \mathbf{B} = \frac{\partial \mathrm{B}_x}{\partial x} + \frac{\partial \mathrm{B}_y}{\partial y} + \frac{\partial \mathrm{B}_z}{\partial z} = 0. \tag{4.8}$$

For this to be true,

$$\frac{\partial \mathrm{B}_x}{\partial x} = -\frac{\partial \mathrm{B}_y}{\partial y} - \frac{\partial \mathrm{B}_z}{\partial z}. \tag{4.9}$$

Also, Ampére's Law states [12],

$$\nabla \times \mathbf{B} = \left(\frac{\partial \mathrm{B}_z}{\partial y} - \frac{\partial \mathrm{B}_y}{\partial z}\right)\mathbf{e}_x + \left(\frac{\partial \mathrm{B}_x}{\partial z} - \frac{\partial \mathrm{B}_z}{\partial x}\right)\mathbf{e}_y + \left(\frac{\partial \mathrm{B}_y}{\partial x} - \frac{\partial \mathrm{B}_x}{\partial y}\right)\mathbf{e}_z = \mu_0 \mathbf{J}. \tag{4.10}$$

The current density, $\mathbf{J} = \mathbf{0}$, except perhaps within the wire of the solenoid, which leads to

$$\frac{\partial \mathrm{B}_y}{\partial x} = \frac{\partial \mathrm{B}_x}{\partial y}, \qquad \frac{\partial \mathrm{B}_z}{\partial x} = \frac{\partial \mathrm{B}_x}{\partial z}, \qquad \frac{\partial \mathrm{B}_z}{\partial y} = \frac{\partial \mathrm{B}_y}{\partial z}. \tag{4.11}$$

With the magnetic field solved in all relevant directions,

$$(\mathbf{B}\cdot\nabla)\mathbf{B} = \begin{pmatrix} -\mathrm{B}_x\left(\dfrac{\partial \mathrm{B}_y}{\partial y}+\dfrac{\partial \mathrm{B}_z}{\partial z}\right)+\mathrm{B}_y\dfrac{\partial \mathrm{B}_x}{\partial y}+\mathrm{B}_z\dfrac{\partial \mathrm{B}_x}{\partial z} \\ \mathrm{B}_x\dfrac{\partial \mathrm{B}_x}{\partial y}+\mathrm{B}_y\dfrac{\partial \mathrm{B}_y}{\partial y}+\mathrm{B}_z\dfrac{\partial \mathrm{B}_y}{\partial z} \\ \mathrm{B}_x\dfrac{\partial \mathrm{B}_x}{\partial z}+\mathrm{B}_y\dfrac{\partial \mathrm{B}_y}{\partial z}+\mathrm{B}_z\dfrac{\partial \mathrm{B}_z}{\partial z} \end{pmatrix}. \tag{4.12}$$

With the form of $(\mathbf{B}\cdot\nabla)\mathbf{B}$, Eq. (3.6) can be efficiently computed and the total force on each cell determined. Note that the accuracy of the discretization can be validated by comparing the estimates for $\partial \mathrm{B}_y/\partial z = \partial \mathrm{B}_z/\partial y$ in that $\mathrm{B}_y(\mathbf{X}_{i,j,k}+\epsilon\mathbf{e}_z) \simeq \mathrm{B}_z(\mathbf{X}_{i,j,k}+\epsilon\mathbf{e}_y)$.

Numerically Solving the ODE

To solve the spatially varying ODE,

$$\frac{\mathrm{d}}{\mathrm{d}t}\mathbf{X} = -\mathbf{e}_z + \Gamma(N_\mathrm{b})\frac{\chi_\mathrm{bead}}{\rho_\mathrm{b}\mu_0}\left(\mathbf{B}\cdot\nabla\right)\mathbf{B}, \tag{4.13}$$

which is (3.25) with $\mathrm{M}_0 = 0$ and dropping the tildes, the magnetic force must be solved at every location the ODE is solved. The spatially varying ODE (4.13) is dependent on the parameter $\Gamma(N_\mathrm{b})\chi_\mathrm{bead}/\rho_\mathrm{b}\mu_0$. Table 3.1 has a variety of parameters that are estimated based off experimental values that are used with (3.16) to estimate this value. It is largely the accuracy of the number of beads found in the cell, N_b, and the magnetic susceptibility of the beads, χ_bead, that affect the resulting trajectory. From a given initial position, $\mathbf{X}(0) = \mathbf{X}_0 = \langle x_0, y_0, z_0\rangle$, the weighted gradient of the field is solved as in the previous subsection, and the total magnetic force felt by the object at the current location is calculated.

Solving the ODE gives a full trajectory of the object in motion. Figure 4.4 shows

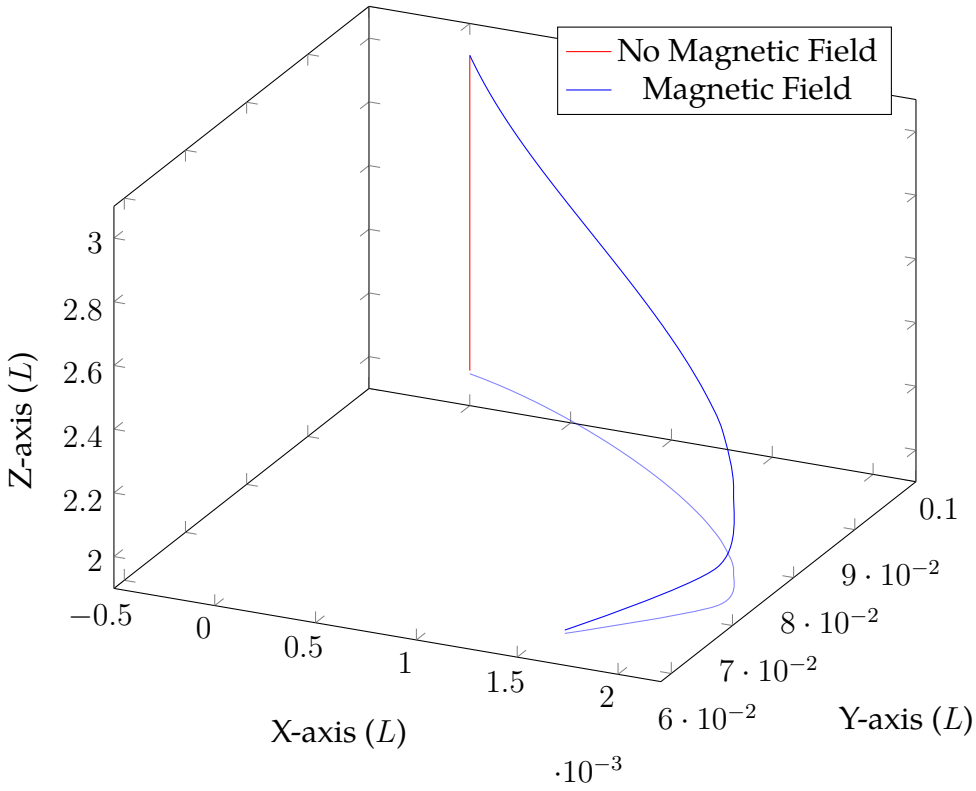

Figure 4.4: Trajectory of a single cell, with and without a magnetic field present. The magnetic field is generated using the same parameters used in the field calculation in Figure 3.6.

the trajectory a cell at an initial location of $\mathbf{X}_0 = \langle 0, 0.1, 2pn+1 \rangle$ will experience with a magnetic field turned on, and turned off. The starting height of the cell, $2pn + 1$, is calculated to be a unit distance of 1 above the top of the solenoid, and is moved a distance of 0.1 away from the origin to accentuate the non-linear affect on the trajectory the magnetic field has.

ODEint

The ODE is solved using SciPy's ODEint tool [35]. ODEint is found in the `scipy.integrate` module. ODEint is based on the LSODA solver of the FORTRAN 77 ODEPACK suite of routines. The method dynamically monitors data to decide when to switch between a non-stiff solver using an Adams predictor-corrector technique to a stiff solver based on backwards differentiation methods. The non-stiff method is tried initially. This set of routines is beneficial due to its ease of implementation within the Python environment and it's flexibility when solving systems with unknown dynamics.

Usage

To use `scipy.integrate.odeint`, a function must be defined. This function will return the $\mathbf{e}_x, \mathbf{e}_y$ and $\mathbf{e}_z$ components of the ordinary differential equation. In the non-dimensionalized model for the motion of the cell, with no magnetic field present, we have the differential equation

$$\frac{\mathrm{d}}{\mathrm{d}t}\mathbf{X}_c = -\mathbf{e}_z. \tag{4.14}$$

This can be defined as the function:

Line	Hits	% Time	Code
81			`@profile`
82			`def find_BdotGradB(pos):`
83	966	0.0	`    h = np.pi*R/N`
84			
85	966	19.9	`    Bx, By, Bz = find_B(pos, theta, R, N, wr)`
86			
87	966	20.0	`    Bx_right, By_right, Bz_right = find_B(pos + [0,h,0], theta, R, N, wr)`
88	966	20.0	`    Bx_left, By_left, Bz_left = find_B(pos - [0,h,0], theta, R, N, wr)`
89	966	20.1	`    Bx_up, By_up, Bz_up = find_B(pos + [0,0,h], theta, R, N, wr)`
90	966	20.0	`    Bx_down, By_down, Bz_down = find_B(pos - [0,0,h], theta, R, N, wr)`
91			
92	966	0.0	`    bxy = (Bx_right - Bx_left) / 2*h`
93	966	0.0	`    byy = (By_right - By_left) / 2*h`
94	966	0.0	`    bzy = (Bz_right - Bz_left) / 2*h`
95			
96	966	0.0	`    bxz = (Bx_up - Bx_down) / 2*h`
97	966	0.0	`    byz = (By_up - By_down) / 2*h`
98	966	0.0	`    bzz = (Bz_up - Bz_down) / 2*h`
99			
100			`    # X derivatives calculated by divergence and curl of B`
101	966	0.0	`    bxx = -byy - bzz`
102	966	0.0	`    byx =  bxy`
103	966	0.0	`    bzx =  bxz`
104	966	0.0	`    return [Bx*bxx + By*bxy + Bz*bxz, Bx*byx + By*byy + Bz*byz, Bx*bzx + By*bzy + Bz*bzz]`
		100	

Table 4.1: Line-by-line profiler of the `find_BdotGradB` function. The entirety of the time spent computing this function is on calculating the field.

```
\def f(X0,t):
    x = 0
    y = 0
    z = -1
    return [x, y, z]
```

where `X0` is the position of the object, and `t` is a vector of times where the solution is solved. To find the solution, `scipy.integrate.odeint` is called. The full solution for the trajectory of the cell using `scipy.integrate.odeint` can be found in Appendix B.

Efficiency of the Numerical Solver

To solve for the magnetic force in this manner is inefficient. Using a line-by-line profiler for Python [36], the time intensive computations are determined. Within

Line	Hits	% Time	Code
68			`@profile`
69			`def find_B(pos, theta, R, N, wr):`
70	4830	0.0	`    cross = 0`
71	4830000	0.8	`    for k in range(1, theta.size):`
72	4825170	3.0	`        rs = np.array([R*np.cos(theta[k]-np.pi/N),`
73	4825170	2.4	`                       R*np.sin(theta[k]-np.pi/N),`
74	4825170	4.0	`                       (p*(theta[k]-np.pi/N))/np.pi])`
75	4825170	1.6	`        r = pos - rs`
76	4825170	3.6	`        dl = np.array([R*(np.cos(theta[k])-np.cos(theta[k-1])),`
77	4825170	3.2	`                       R*(np.sin(theta[k])-np.sin(theta[k-1])),`
78	4825170	2.5	`                       p/N])`
79	4825170	79.0	`        cross += C * np.cross(dl, r) / LA.norm(r)**3`
80	4830	0.0	`    return cross`
		100.1	

Table 4.2: Line-by-line profiler of the `find_B` function. The majority of the time spend calculating the field is spent computing the cross product summed over all segments of the solenoid.

the trajectory program (B), the bulk of the time spent computing the trajectory is in the calculation of the magnetic field. This can be seen in Table 4.1, where 100% of the time spent in the function `find_bDotGradB` is used by the five calls to the `find_B` function.

When examining the cause of the long time spent in the `find_B` function using the line-by-line profiler, a single line stands out. When at a given location $\mathbf{X}_{i,j,k}$, the normalized cross product $\Delta\mathbf{l}(\theta_m) \times \mathbf{r}_m/\|\mathbf{r}_m\|^3$ must be calculated once for each segment of the solenoid as seen in (4.7). With n coils in the solenoid, and N segments per coil, this results in nN calculations at every new position.

To improve the efficiency of the magnetic field computation, a component-wise calculation can be done for the cross product (see Appendix C for list of relevant cross products), with the result that

$$\begin{aligned}\Delta\mathbf{l}_m \times \mathbf{r}_m = &\left(a(1-\cos(\Delta\theta))\hat{\mathbf{r}}_m + a\sin(\Delta\theta)\hat{\theta}_m + \frac{p}{N}\mathbf{e}_z\right) \times \\ &\left(\langle x_i, y_j, 0\rangle - a\cos\left(\frac{1}{2}\Delta\theta\right)\hat{\mathbf{r}}_m \right. \\ &\left. + a\sin\left(\frac{1}{2}\Delta\theta\right)\hat{\theta}_m + \left(z_k - \frac{p}{2N}(2m-1)\right)\mathbf{e}_z\right).\end{aligned} \tag{4.15}$$

The simplified components are given by

$$
\begin{aligned}
(\Delta\mathbf{l}_m \times \mathbf{r}_m) \cdot \mathbf{e}_x &= a\left(z_k - \frac{p}{2N}(2m-1)\right)(\sin\theta_m - \sin\theta_{m-1}) \\
&\quad - \frac{p}{N}\left(y_j - a\sin\left(\theta_m - \frac{1}{2}\Delta\theta\right)\right), \qquad (4.16a) \\
(\Delta\mathbf{l}_m \times \mathbf{r}_m) \cdot \mathbf{e}_y &= -a\left(z_k - \frac{p}{2N}(2m-1)\right)(\cos\theta_m - \cos\theta_{m-1}) \\
&\quad + \frac{p}{N}\left(x_i - a\cos\left(\theta_m - \frac{1}{2}\Delta\theta\right)\right), \qquad (4.16b) \\
(\Delta\mathbf{l}_m \times \mathbf{r}_m) \cdot \mathbf{e}_z &= -ax_i(\sin\theta_m - \sin\theta_{m-1}) \\
&\quad + ay_j(\cos\theta_m - \cos\theta_{m-1}) \\
&\quad + 2a^2\sin\left(\frac{1}{2}\Delta\theta\right). \qquad (4.16c)
\end{aligned}
$$

A similar method can be used to determine $\|\mathbf{r}_m\|^3 = (\mathbf{r}_m \cdot \mathbf{r}_m)^{3/2}$, where $\mathbf{r}_m \cdot \mathbf{r}_m$ is the 2-norm,

$$
\begin{aligned}
\mathbf{r}_m \cdot \mathbf{r}_m &= \Bigg\| \langle x_i, y_j, 0\rangle - a\cos\left(\frac{1}{2}\Delta\theta\right)\hat{\mathbf{r}}_m \\
&\qquad + a\sin\left(\frac{1}{2}\Delta\theta\right)\hat{\theta}_m + \left(z_k - \frac{p}{2N}(2m-1)\right)\mathbf{e}_z \Bigg\|^2 \\
&= \left(x - a\cos\left(\theta_m - \frac{1}{2}\Delta\theta\right)\right)^2 + \left(y - a\sin\left(\theta_m - \frac{1}{2}\Delta\theta\right)\right)^2 \\
&\qquad + \left(z - \frac{p}{2N}(2m-1)\right)^2. \qquad (4.17)
\end{aligned}
$$

In order to compare computation efficiency, the component-wise computation was implemented into a second function, `find_B_v2`.

CHAPTER 5

Results

During the simulation, cells with engulfed beads are modeled as a single entity. As such, any effects the beads have on the cells are ignored. Important insight can be gained from these simulations including the time required to reach the base of the cell culture dish, the translocation time of the cell, and the trajectory the cell takes during this journey. When computing the translocation times and trajectories of a cell with magnetic bead(s) engulfed within, as in Figure 4.4, an initial starting position of the cell must be provided to the numerical solver. In the results that follow, the translocation times and positions are nondimensional. As in Section 3.2, a length scale of L and a time scale of T are implied.

Translocation Time

For an initial starting position of $\mathbf{X}_0 = \langle 0, 0.1, 2pn + 1 \rangle$, as in Figure 4.4, the nondimensional time required for the cell, in the presence of an applied magnetic field, to translocate to base of the cell culture dish is roughly 40% of the time required for

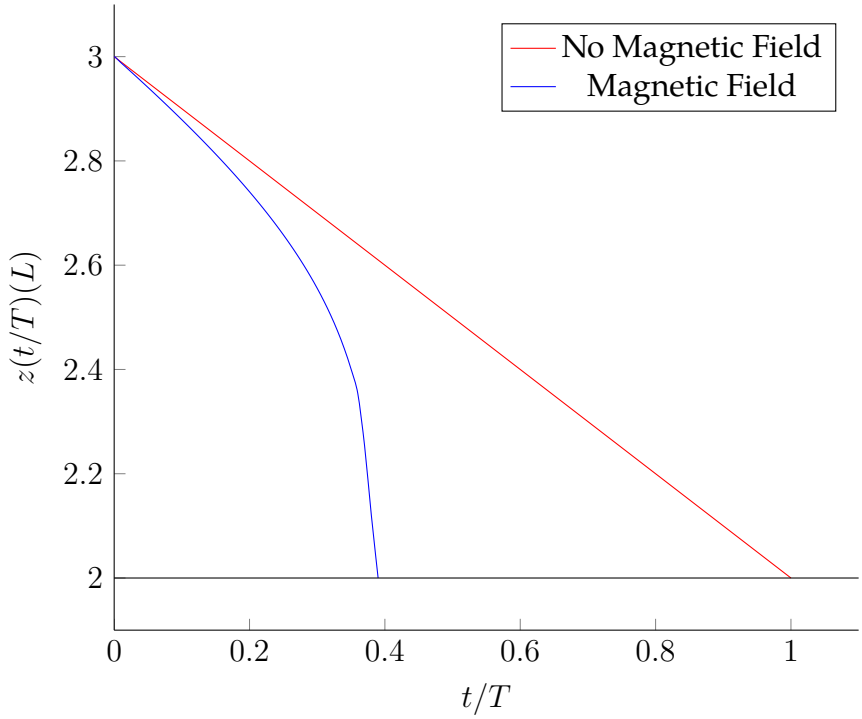

Figure 5.1: The nondimensional time required for a cell to fall from the top of the cell culture dish to the bottom. When a magnetic field is present, the time is drastically reduced. The ratio between the time with no magnetic field applied to with a magnetic field applied can be tuned to match expected results by modifying the magnetic field.

a cell to translocate when there is no field applied. The height above the base of the dish at each time step is shown in Figure 5.1.

To examine the affects the magnetic field has on the trajectory of the cells, cells have been placed in various initial positions. Placing cells along the $x = y$ plane at a height of $z = 2pn + 1$, at various distances from the centre of the solenoid, the time required for the cell to translocate increases as the distance increases. For distances from the centre of the solenoid ranging from $R/L = 0.07$ to 0.56, times increase from $t/T = 0.4$ to 0.6, as seen in Figure 5.2.

To understand the relationship between the distance to the centre of the solenoid and the time for the cell to fall, the trajectories for cells placed at various points around the solenoid are tracked, and their times compared. At a distance of $R/L = 0.25$, half way from the centre of the solenoid to the coils, twelve cells are released

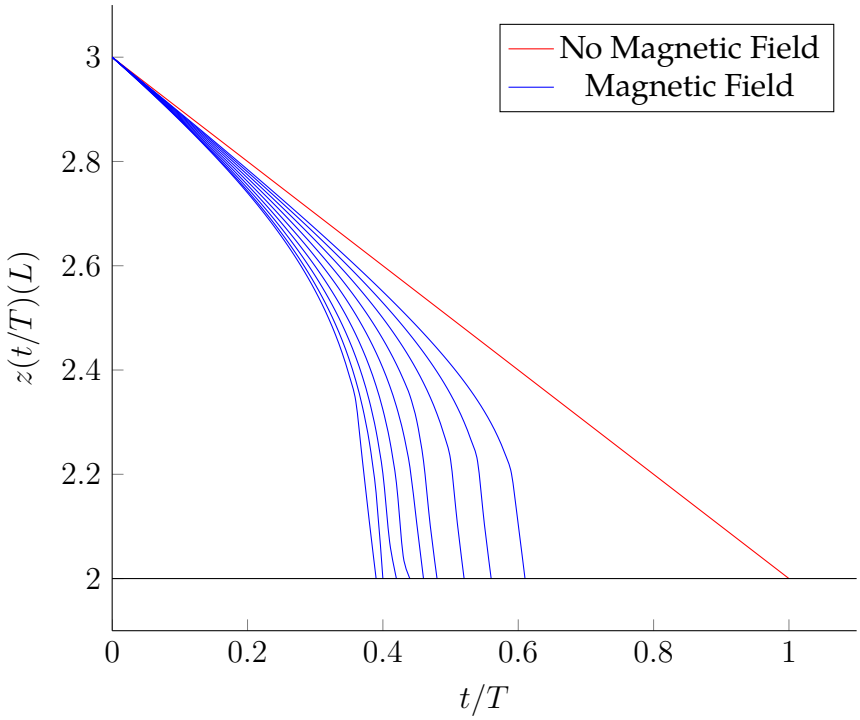

Figure 5.2: Translocation times for multiple cells to fall to the base of the dish. When the cells have a starting location close to the centre of the solenoid, the time required to reach the base of the dish is shortest. Shown are times from starting positions ranging from $R/L \sim 0.07$ to ~ 0.56 away from the centre of the solenoid, along the line $x = y$.

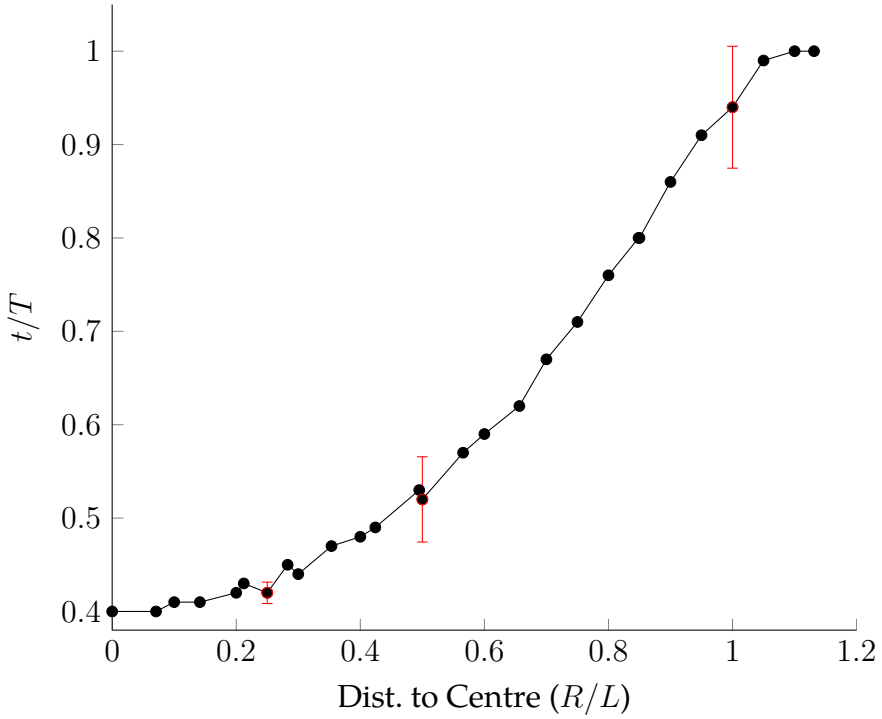

Figure 5.3: Translocation times for multiple cells to fall to the base of the dish. For cells released within a close proximity to the centre or the solenoid, $R/L < 0.1$, a time of 0.4 is observed. As the distance from the centre increases to the radius of the solenoid, $R/L = 0.5$, the time required to reach the base increases, and there is a larger standard deviation (red). At distances well outside of the range of the magnetic field, $R/L > 1$, the times for the cell to fall approaches the time for a cell to fall without an applied magnetic field.

around the solenoid. The standard deviation of the times is calculated, and is shown in Figure 5.3. This process is repeated at a distance of $R/L = 0.5$, directly above the coils, and $R/L = 1.0$, well outside of the solenoid. As cells are released from positions farther from the centre of the solenoid, the time required to reach the base of the dish approach the time required for a cell without an applied magnetic field. This behaviour is expected, as **B** is more uniform, and decreases drastically, as the distances from the solenoid increases.

During the loading process, the cells engulf different numbers of beads. It was shown in Section 3.2 that $\Gamma(N_\mathrm{b})$ is linearly dependant to the number of beads, N_b, in a cell. To understand how the speed of translocation for the cell is affected by

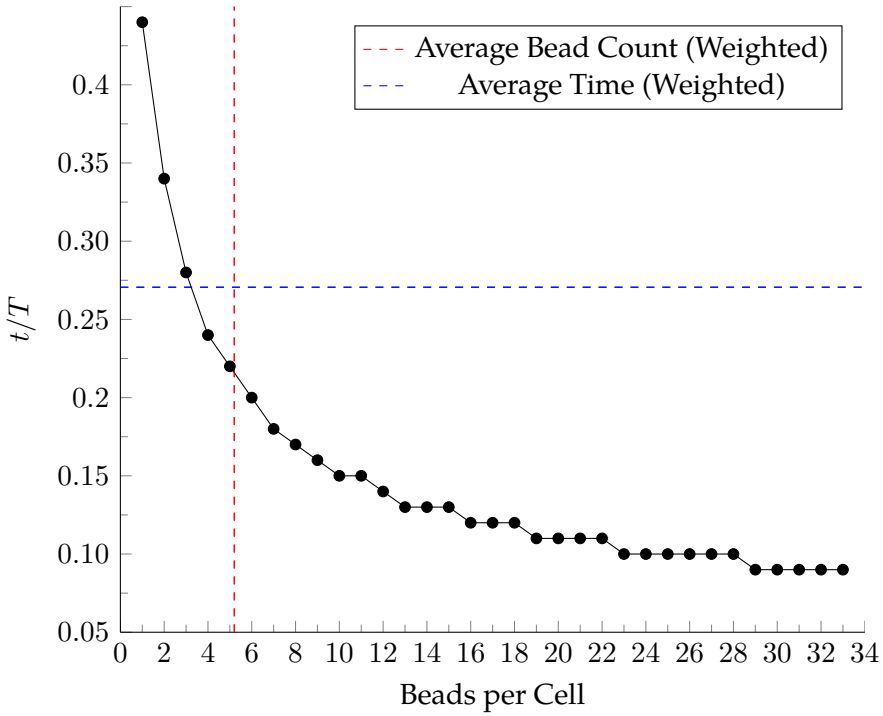

Figure 5.4: The translocation time for cells with between 1 and 33 magnetic beads engulfed. The average count of the beads as well as the average time to the base of the dish, weighted by the frequency in Figure 3.3, is shown. Plateauing, which can be observed here, occurs when the time-step of the numerical ODE solver is too large.

a varying number of beads, cells are released from $\mathbf{X}_0 = \langle 0, 0, 2pn + 1 \rangle$, with N_b ranging from 1 to 33. The relationship between the number of magnetic beads found in each cell and the time to reach the bottom of the dish is not linear, seen in Figure 5.4. This is largely due to the non-linearity of the equation of motion for the cell, (3.25). The vertical trajectories and the times required to reach the base can be seen in Figure 5.5.

Using the frequency distribution of the number of magnetic beads found in each cell, shown in Figure 3.3, it is possible to determine the expected times for cells released from a given position. For the given distribution, the average time is determined to be $t/T = 0.22$, and the frequency of cells taking a given time can be approximated by the trend line in Figure 5.6.

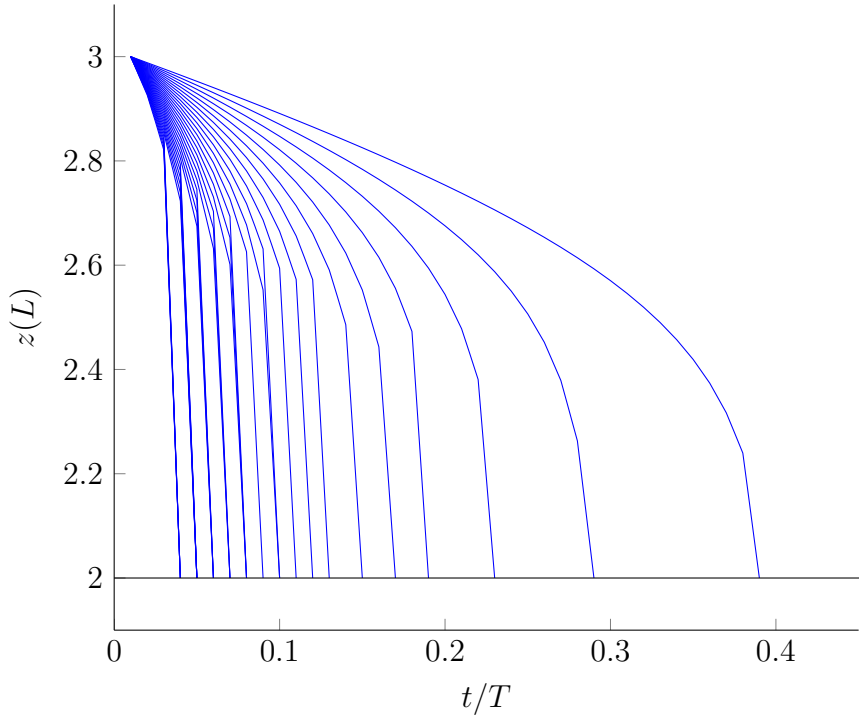

Figure 5.5: The time required for cells to reach the base of the dish with bead counts from 1 to 33. The $\mathbf{e}_z$ component to the trajectories is displayed.

Trajectories

Figure 4.4 shows the trajectory of the cells is not purely radial. There is an azimuthal component to the motion. The trajectories of multiple cells, all with a single magnetic bead within, is shown in Figure 5.7. Cells are released from positions along the $x = y$ plane at a height of $z = 2pn + 1$, at distances from the centre of the solenoid ranging from $R/L = 0.07$ to $R/L = 0.56$. Cells that are released from positions close to the centre of the solenoid experience a larger azimuthal component to the motion, best observed in Figure 5.7a, but minimal radial motion. However, when cells are released from positions further from the solenoid, the radial component takes over, and the cells are pulled towards the solenoid, as seen in Figure 5.7b.

If cells are placed further, the strength of the applied magnetic field is minimal. This causes the cells to experience little radial and azimuthal motion. Figure 5.8 ex-

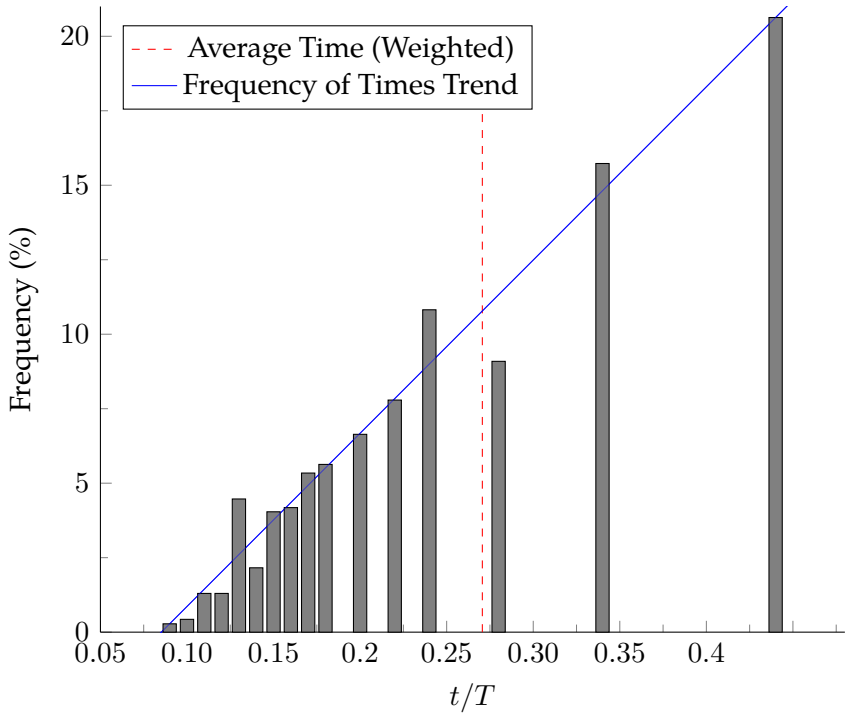

Figure 5.6: Using the distribution of the number of beads found in each cell seen in Figure 3.3, the frequency of various times to translocate to the base of the dish is determined.

amines a variety of cells released from a position within the radius of the solenoid, as well as cells released as far as $R/L = 1.0$. At $R/L = 1.0$, the cells are not pulled within the radius of the solenoid.

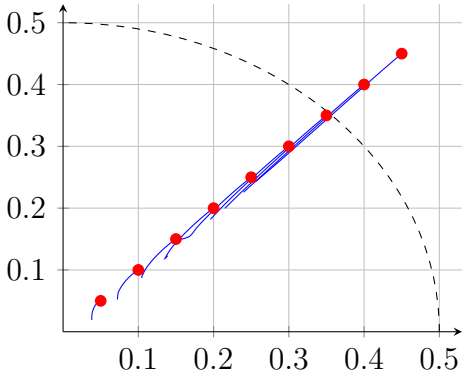

(a) Top down view of cell starting positions (red) and their trajectories.

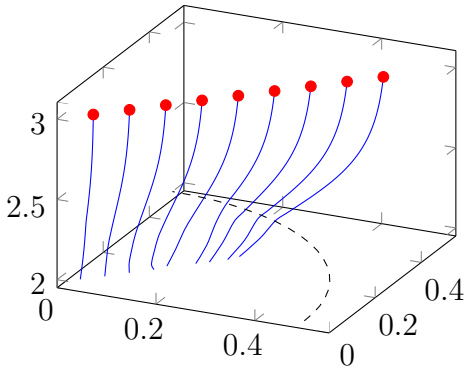

(b) View of cell starting positions (red) and their trajectories in 3D.

Figure 5.7: Trajectories of cells close to the centre of the solenoid experience a force in the azimuthal direction than cells further from the centre of the solenoid. This is due in part to a minimal radial component to the force at positions within the solenoid. At positions near the loops of the solenoid, the radial component is predominant. All lengths are in units of L.

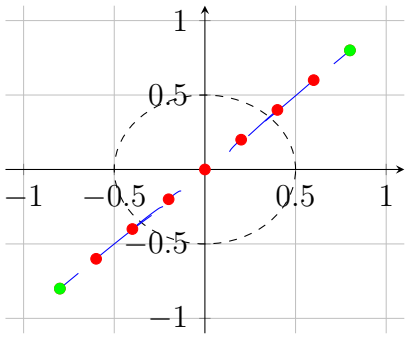

(a) Top down view of cell starting positions (red/green) and their trajectories.

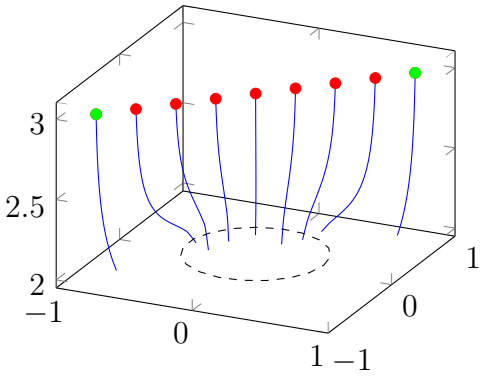

(b) View of cell starting positions (red/green) and their trajectories in 3D.

Figure 5.8: Trajectories of cells far from the centre of the solenoid. When the starting positions of the cells becomes further from the solenoid (green), the radial component of the force generated by the solenoid is not strong enough to pull the cell towards it. All lengths are in units of L.

CHAPTER 6

Conclusion

One method for the growth of tissue in a controlled environment is the colonization of porous scaffolds with cells. Once these scaffolds are seeded with cells, the tissue can be used for a variety of applications. In order to efficiently grow tissue in this manner, it is important to understand how the cells move throughout the system. With the addition of magnetic particles, the cells reach the scaffold quicker than with gravity alone. The model developed in this project uses superparamagnetic particles engulfed within the cells to control their movement in an applied magnetic field. Portions of the work presented in this dissertation has appeared in a peer reviewed conference proceeding [37, 38].

The equation of motion relies on three main forces: gravity, friction and magnetism. The force applied to the cell due to gravity is exclusively in the $\mathbf{e}_z$ direction, while the force of friction is applied opposite to the velocity of the cell. The magnetic force is dependant on the applied magnetic field.

When the cells engulf the magnetic particles by phagocytosis, a distribution of magnetic particles within the cells is observed. The varying number of magnetic

particles within each cell changes the force that the cell experiences when a magnetic field is applied. It is determined in this project that the magnetic force is linearly related to the number of magnetic particles in the cell.

It is determined that the cells motion can be described by

$$\frac{\mathrm{d}}{\mathrm{d}t}\mathbf{X} = -\mathbf{e}_z + \Gamma(N_\mathrm{b})\left(\left(\frac{\mathsf{M}_0}{B_0}\cdot\nabla\right)\mathbf{B} + \frac{\chi_\mathrm{bead}}{\rho_\mathrm{b}\mu_0}(\mathbf{B}\cdot\nabla)\mathbf{B}\right)$$

where the effect of inertia is disregarded and $\Gamma(N_\mathrm{b})$ depends on a number of physical parameters. In order to solve this equation of motion, a magnetic field must be computed. Using a solenoid placed below the cell culture dish, a magnetic field is computed that creates a force towards the centre of the solenoid.

To compute the magnetic field numerically, the solenoid is discretized. With a discretized solenoid, it is possible to compute the applied magnetic field at any position to which the cell travels. Furthermore, it is possible to generate the magnetic field a single time, and change the orientation of the solenoid or collection of solenoids to determine the total field. At each of the positions the magnetic field is generated, the magnetic force is computed. The differential equation for the equation of motion can then be solved.

When solving the differential equation at initial positions which are close to directly above the centre of the solenoid and with a single magnetic particle within the cell, the time required for the cells to translocate and reach the base of the cell culture dish is minimized. Therefore it is crucial to place the cells as close to the centre of the solenoid as possible in order to seed the scaffold in a minimal amount of time.

Examining the trajectories of the cells released from positions within the radius of the solenoid and from outside of it emphasizes the need to position cells above the centre of the solenoid. When the cells are too far away from the solenoid, the

radial component to the forces is not strong enough to have a substantial effect on the trajectories, and the cell will land outside of the solenoid's radius.

Furthermore, when the initial positions are further from the centre of the solenoid, the times required to translocate fluctuate. The fluctuation of times is due to the lack of symmetry in the solenoid design. If the solenoid was modeled as an ideal solenoid, with infinitesimally thin wires and no pitch, the fluctuation would not occur. This indicates cells should be released from positions close to the centre of the solenoid to ensure a proper time of translocation can be determined.

Control over the final position of the cells is needed to ensure the cells are captured by the scaffold. The use of a larger solenoid would allow for a larger scaffold to be contained within the area of highest density cell collection.

Future Work

The goal of this work is to model the movement of cells for the purpose of tissue engineering. A critical part in the tissue engineering process is the seeding of these cells onto porous scaffolds. A hazard function can be used to simulate the adhering process that takes place between the cells and the scaffold. Doing so would yield a more accurate model for use in bio-medicine.

With a varying number of magnetic particles within each cell, it may be possible to sort the beads prior to seeding the cells onto the scaffold. The sorting process must be completed before the first cells reach the base of the dish. This would allow greater control over the positions of the cells, as well as the time required for the cells to reach the scaffold.

It may also be useful to control the final position of the cells within a potentially thick scaffold in order to create more complex tissue structures. In order to accomplish this, two or more solenoids could be of use. The majority of the force

for a single solenoid is applied in the direction towards the solenoid. With multiple solenoids along perpendicular axes, it could be possible to control the position of the cells by fluctuating the current in each of the solenoids. These techniques can lead to the development and seeding of scaffolds for use in the creation of more complex tissue structures.

Bibliography

[1] G. A. Villalona, B. Udelsman, D. R. Duncan, E. McGillicuddy, R. F. Sawh-Martinez, N. Hibino, C. Painter, T. Mirensky, B. Erickson, T. Shinoka, and C. K. Breuer, "Cell-Seeding Techniques In Vascular Tissue Engineering," *Tissue Engineering*, vol. 16, no. 3, pp. 341–350, 2010.

[2] S. S. Shevkoplyas, A. C. Siegel, R. M. Westervelt, M. G. Prentiss, and G. M. Whitesides, "The Force Acting on a Superparamagnetic Bead Due To an Applied Magnetic Field." *Lab on a chip*, vol. 7, no. 10, pp. 1294–1302, 2007.

[3] T. Fallesen, D. B. Hill, M. Steen, J. C. Macosko, K. Bonin, and G. Holzwarth, "Magnet Polepiece Design For Uniform Magnetic Force on Superparamagnetic Beads," *Review of Scientific Instruments*, vol. 81, 2010.

[4] I. Šafařík and M. Šafaříková, "Use of Magnetic Techniques For the Isolation of Cells," *Journal of Chromatography B: Biomedical Sciences and Applications*, vol. 722, no. 1-2, pp. 33–53, 1999.

[5] K. Shimizu, A. Ito, and H. Honda, "Enhanced Cell-Seeding Into 3D Porous Scaffolds By Use of Magnetite Nanoparticles," *Journal of Biomedical Materials Research - Part B Applied Biomaterials*, vol. 77, no. 2, pp. 265–272, 2006.

[6] J. Dobson, "Remote Control of Cellular Behaviour With Magnetic Nanoparticles." *Nature Nanotechnology*, vol. 3, no. 3, pp. 139–143, 2008.

[7] J. L. Corchero and A. Villaverde, "Biomedical Applications of Distally Controlled Magnetic Nanoparticles," *Trends in Biotechnology*, vol. 27, no. 8, pp. 468–476, 2009.

[8] X. Jin, Y. Zhao, A. Richardson, L. Moore, P. S. Williams, M. Zborowski, and J. J. Chalmers, "Differences In Magnetically Induced Motion of Diamagnetic, Paramagnetic, and Superparamagnetic Microparticles Detected By Cell Tracking Velocimetry." *The Analyst*, vol. 133, no. 12, pp. 1767–75, 2008.

[9] J. Xu, K. Mahajan, W. Xue, J. O. Winter, M. Zborowski, and J. J. Chalmers, "Simultaneous, Single Particle, Magnetization and Size Measurements of Micron Sized, Magnetic Particles," *Journal of Magnetism and Magnetic Materials*, vol. 324, no. 24, pp. 4189–4199, 2012.

[10] J. L. Semple, N. Woolridge, and C. J. Lumsden, "In Vitro, In Vivo, In Silico: Computational Systems In Tissue Engineering and Regenerative Medicine," *Tissue Engineering*, vol. 11, no. 3, pp. 341–356, 2005.

[11] A. Robu, L. Stoicu-Tivadar, and N. Robu, "Computational Study of the Potential Role of Chemotaxis In Enhancing the Cell Seeding of Tissue Engineering Scaffolds," 2014.

[12] P. Lorrain and D. Corson, *Electromagnetic Fields and Waves*. San Francisco CA: W. H. Freeman and Company, 1970.

[13] P. T. Leung, "A Note on the *System-Free* Expressions of Maxwell's Equations," *European Journal of Physics*, vol. 25, no. 2, p. N1, 2003.

[14] J. Farley and R. H. Price, "Field Just Outside a Long Solenoid," *American Journal of Physics*, vol. 69, no. 7, p. 751, 2001.

[15] M. A. Armoogam, "Electro-Mechanical Locking Mechanism," 1993. [Online]. Available: https://www.google.com/patents/US5216909

[16] L. Bauer, J. Semler, M. Krohn, and F. Schlitzer, "Arrangement of Solenoid Valves, a Central Plug and a Printed Circuit Board on a Control Housing of an Automatic Shift Device of a Toothed-wheel Variable-speed Gearbox," 1997. [Online]. Available: https://www.google.com/patents/US5611372

[17] R. Reinicke, "Solenoid operated valve with magnetic latch," 1974. [Online]. Available: https://www.google.com/patents/US3814376

[18] J. Thomas, D. Jones, L. Moldovan, K. Gooch, and N. Moldovan, "Labeling of Endothelial Cells By Phagocytosis of Micron-Sized Beads For Magnetic Force-Assisted Colonization of Fibrillar Scaffolds. Unpublished Manuscript," pp. 1–33, 2018.

[19] C. Kittle, *Introduction To Solid State Physics*, 2nd ed. New York: John Wiley & Sons, Inc, 1962.

[20] M. Gottlieb and R. Pfeiffer, "The Feynman Lectures on Physics Vol. II Ch. 34: The Magnetism of Matter," 2013.

[21] M. Knobel, W. C. Nunes, L. M. Socolovsky, E. D. Biasi, J. M. Vargas, and J. C. Denardin, "Superparamagnetism and Other Magnetic Features In Granular Materials : A Review on Ideal and Real Systems," 2008.

[22] C. P. Bean and J. D. Livingston, "Superparamagnetism," *Journal of Applied Physics*, vol. 30, no. 4, pp. S120–S129, 1959.

[23] Miltenyi Biotec, "Miltenyi Biotec." [Online]. Available: http://www.miltenyibiotec.com

[24] ——, "MACS MicroBeads." [Online]. Available: http://www.miltenyibiotec.com/en/products-and-services/macs-cell-separation/macs-technology/microbeads{_}dp.aspx

[25] ——, "Anti-Biotin MACSiBead Particles." [Online]. Available: http://www.miltenyibiotec.com/{~}/media/Images/Products/Import/0001100/IM0001142.ashx?force=1

[26] "ScienCell." [Online]. Available: https://www.sciencellonline.com/

[27] ScienCell, "Human Umbilical Vein Endothelial Cells," pp. 1–2. [Online]. Available: https://www.sciencellonline.com/PS/8000.pdf

[28] S. Jewett, *Physics For Scientists and Engineers*, 6th ed. Belmont CA: Brooks/Cole–Thomson Learning, 2004.

[29] N. Moldovan, "Indiana University–Purdue University Indianapolis," personal communication.

[30] O. Espinosa and V. Slusarenko, "The Magnetic Field of an Infinite Solenoid," *American Journal of Physics*, vol. 71, no. 9, p. 953, 2003.

[31] B. B. Dasgupta, "Magnetic Field Due To a Solenoid," *American Journal of Physics*, vol. 52, no. 3, p. 258, 1984.

[32] S. Basu, S. S. Pany, P. Bannerjee, and S. Mitra, "Pulsed Magnetic Field Measurement Outside Finite Length Solenoid : Experimental Results & Mathematical Verification," vol. 2013, no. October, pp. 371–378, 2013.

[33] A. I. Rusinov, "High Precision Computation of Solenoid Magnetic Fields By Garrett's Methods," *IEEE Transactions on Magnetics*, vol. 30, no. 4, pp. 2685–2688, 1994.

[34] V. Labinac, N. Erceg, and D. Kotnik-Karuza, "Magnetic Field of a Cylindrical Coil," *American Journal of Physics*, vol. 74, no. 7, p. 621, 2006.

[35] E. Jones, T. Oliphant, P. Peterson *et al.*, "SCIPY: Open Source Scientific Tools For Python," 2001–. [Online]. Available: http://www.scipy.org/

[36] R. Kern, "Line_profiler For Python." [Online]. Available: https://github.com/rkern/line_profiler

[37] D. J. Pasut, "Modelling the Movement of Superparamagnetic Beads Engulfed In Endothelial Cells," 2017, Applied Mathematics, Modeling and Computational Science (AMMCS). [Online]. Available: http://www.ammcs2017.wlu.ca/static/files/AMMCS2017-Book-of-Abstracts.pdf

[38] D. J. Pasut and C. S. Bohun, "Modelling the Movement of Superparamagnetic Beads Engulfed In Endothelial Cells," *Journal of Coupled Systems and Multiscale-Dynamics*, vol. 5, no. 4, 2017.

Appendices

APPENDIX A

Code: Field Calculation on Uniform Grid

```
#!/usr/bin/env python
# Author: Daniel Pasut <daniel.pasut@uoit.net>
# (c) 2018

import numpy as np
#import seaborn as sns
import matplotlib.pyplot as plt
from mpl_toolkits.mplot3d import Axes3D
from numpy import linalg as LA
from pylab import *
from tqdm import tqdm
import sys

gs = 30  # Grid spacing
R = 0.5  # Radius of loop (cm)
wr = 0.1  # Radius of wire (mm)
p = 0.1  # Pitch of wire, centre-to-centre (mm)
N = 100  # Number of segments in single loop of wire
n = int(sys.argv[1])#1  # Number of loops of wire
theta = np.empty(n*N)
mu = 1  # Magnetic susceptibility
I = -1  # Current
C = mu*I/(4*np.pi)
xmin = -2.1
xmax = 2.1
```

```
ymin = -2.1
ymax = 2.1
zmin = -1.1
zmax =  p*n*2+1.1
x = np.linspace(xmin, xmax, gs)  # Positions for x
y = np.linspace(ymin, ymax, gs)  # Positions for y
z = np.linspace(zmin, zmax, gs)  # Positions for z
Y, Z = np.meshgrid(y, z, indexing='ij')  # Grid for y/z
h = (ymax - ymin)/gs
# x's are all zero, looking at plane
Bx = np.zeros([gs, gs])  # x components don't change
By = np.zeros([gs, gs])  # y components of field matrix
Bz = np.zeros([gs, gs])  # z components of field matrix
norms = np.zeros([gs, gs])  # matrix for norms at each point

Fx = np.zeros([gs, gs])
Fy = np.zeros([gs, gs])
Fz = np.zeros([gs, gs])

values = np.zeros([4,gs])
xvals = np.arange(gs)
insidez = 0.


# Function to do summation over all segments of wire
def find_B(pos, theta, R, N, wr):
    cross = 0
    for k in range(1, theta.size):
        rs = np.array([R*np.cos(theta[k]-np.pi/N),
                       R*np.sin(theta[k]-np.pi/N),
                       (p*(theta[k]-np.pi/N))/np.pi])
        r = pos - rs
        dl = np.array([R*(np.cos(theta[k])-np.cos(theta[k-1])),
                       R*(np.sin(theta[k])-np.sin(theta[k-1])),
                       p/N])
        if LA.norm(r) <= 1.35*wr:
            inwire = np.array([0, 0, 0])
            return inwire
        else:
            cross += C * np.cross(dl, r) / LA.norm(r)**3
    return cross


# Plot the solenoid in 3-D
def plot_solenoid():
```

```
    wire = np.array([R*np.cos(theta), R*np.sin(theta), p*theta/np.pi])

    fig = plt.figure(figsize=(20, 16), dpi=600, facecolor='w',
                     edgecolor='k')
    ax = fig.gca(projection='3d')
    ax.plot(wire[0], wire[1], wire[2], label='wire', LineWidth=7)

    ax.set_xlabel('\n' + 'X axis', fontsize=30, linespacing=4)
    ax.set_ylabel('\n' + 'Y axis', fontsize=30, linespacing=4)
    ax.set_zlabel('\n' + 'Z axis', fontsize=30, linespacing=4)
    ax.xaxis._axinfo['label']['space_factor'] = 100

    plt.tick_params(axis='both', which='major', labelsize=30)
    plt.savefig('wire-loop.png', transparent=True,
                bbox_inches='tight', pad_inches=0)


# Calculate the magnetic field and find norms
def find_field():
    for j in tqdm(range(y.size)):
        for k in range(z.size):
            pos = np.array([0, y[j], z[k]])
            Bx[j, k], By[j, k], Bz[j, k] = find_B(pos, theta, R, N, wr)
            norms[j, k] = LA.norm([Bx[j, k], By[j, k], Bz[j, k]])
            if k == z.size/2:
                values[0, j] = Bx[j, k]
                values[1, j] = By[j, k]
                values[2, j] = Bz[j, k]
                values[3, j] = abs(y[j]) - R
                if j == y.size/2:
                    insidez = Bz[j, k]
    return insidez


# Calculate Forces
def find_BdotGradB():
    for j in tqdm(range(1, y.size - 1)):
        for k in range(1, z.size - 1):
            bxy = (Bx[j+1, k] - Bx[j-1, k]) / 2*h
            byy = (By[j+1, k] - By[j-1, k]) / 2*h
            bzy = (Bz[j+1, k] - Bz[j-1, k]) / 2*h

            bxz = (Bx[j, k+1] - Bx[j, k-1]) / 2*h
            byz = (By[j, k+1] - By[j, k-1]) / 2*h
            bzz = (Bz[j, k+1] - Bz[j, k-1]) / 2*h
```

```
            # X derivatives calculated by divergence and curl of B
            bxx = -byy - bzz
            byx =  bxy
            bzx =  - bxz

            Fx[j, k] = Bx[j,k]*bxx + By[j,k]*bxy + Bz[j,k]*bxz
            Fy[j, k] = Bx[j,k]*byx + By[j,k]*byy + Bz[j,k]*byz
            Fz[j, k] = Bx[j,k]*bzx + By[j,k]*bzy + Bz[j,k]*bzz

            pos = np.array([0, y[j], z[k]])

            for q in range(1, theta.size):
                rs = np.array([R*np.cos(theta[q]-np.pi/N),
                       R*np.sin(theta[q]-np.pi/N),
                       (p*(theta[q]-np.pi/N))/np.pi])
                r = pos - rs

                if LA.norm(r) <= 1.25*wr:
                    Fx[j, k] = 0
                    Fy[j, k] = 0
                    Fz[j, k] = 0



# Plot quiver diagram
def plot_field():
    print(By[29])
    with open('goodField.dat','a+') as f:
        f.write("y z u v\n")
        for j in range(size(y)):
            for k in range(size(z)):
                f.write("%.8f %.8f %.8f %.8f\n" %
                        (y[j], z[k], By[j,k], Bz[j,k]))


    fig, ax = plt.subplots(figsize=(20, 16), dpi=600)

    for i in range(n):
        circ = plt.Circle((R*np.sin(np.pi/2), (4*i+1)*p/2), radius=wr,
                          color='k', alpha=0.5)
        ax.add_patch(circ)
        circ = plt.Circle((R*np.sin(3*np.pi/2), (4*i+3)*p/2), radius=wr,
                          color='k', alpha=0.5)
        ax.add_patch(circ)
```

```
            plt.plot(R*np.sin(np.pi/2), (4*i+1)*p/2, '*k', R*np.sin(3*np.pi/2),
                     (4*i+3)*p/2, 'ok')
        ax.quiver(Y, Z, By, Bz)
        ax.set_xlim((ymin, ymax))  # set the xlim to xmin, xmax
        ax.set_ylim((zmin, zmax))

        ax.spines['bottom'].set_color('k')
        ax.spines['top'].set_color('white')
        #ax.set(aspect=1, title='Quiver Plot - field lines')
        plt.xlabel('Y axis', fontsize=30)
        plt.ylabel('Z axis', fontsize=30)
        plt.tick_params(axis='both', which='major', labelsize=30)
        plt.savefig('field-loop-test.png', transparent=True,
                    bbox_inches='tight', pad_inches=0)
        plt.savefig('field-loop-test.jpg', bbox_inches='tight', pad_inches=0)
        plt.show()

    # Plot quiver diagram
    def plot_forces():
        fig, ax = plt.subplots(figsize=(20, 16), dpi=600)

        for i in range(n):
            circ = plt.Circle((R*np.sin(np.pi/2), (4*i+1)*p/2), radius=wr,
                              color='k', alpha=0.5)
            ax.add_patch(circ)
            circ = plt.Circle((R*np.sin(3*np.pi/2), (4*i+3)*p/2), radius=wr,
                              color='k', alpha=0.5)
            ax.add_patch(circ)
            plt.plot(R*np.sin(np.pi/2), (4*i+1)*p/2, 'ok', R*np.sin(3*np.pi/2),
                     (4*i+3)*p/2, '*k')

        ax.quiver(Y, Z, Fy, Fz)
        ax.set_xlim((ymin +0.5, ymax -0.5))  # set the xlim to xmin, xmax
        ax.set_ylim((2*p*n, zmax))
        ax.spines['bottom'].set_color('k')
        ax.spines['top'].set_color('white')
        plt.xlabel('Y axis', fontsize=30)
        plt.ylabel('Z axis', fontsize=30)
        plt.tick_params(axis='both', which='major', labelsize=30)
        ax.set(aspect=1)
        plt.savefig('forces-loop.png', transparent=True,
                    bbox_inches='tight', pad_inches=0)
        plt.savefig('forces-loop.jpg', bbox_inches='tight', pad_inches=0)

    if __name__ == '__main__':
```

```
for i in range(0, theta.size):
    theta[i] = i*2*np.pi/N

plot_solenoid()

insidez = find_field()
find_BdotGradB()

plot_field()
plot_forces()
```

APPENDIX B

Code: Trajectory of Cell

```
#!/usr/bin/env python
# Author: Daniel Pasut <daniel.pasut@uoit.net>
# (c) 2018

import numpy as np
import math
import seaborn as sns
from numpy import linalg as LA
from pylab import *
from tqdm import tqdm
import sys
from scipy.integrate import odeint
from scipy.integrate import ode

# Solenoid
gs = 30  # Grid spacing
R = 0.5  # Radius of loop (mm)
wr = 0.1  # Radius of wire (mm)
p = 0.1  # Pitch of wire, centre-to-centre (mm)
N = 100  # Number of segments in single loop of wire
n = int(sys.argv[1])#1  # Number of loops of wire
theta = np.empty(n*N)
mu = 1  # Magnetic susceptibility
I = 10  # Current
C = mu*I/(4*np.pi)

# Geometry
```

```
xmin = -2.1
xmax = 2.1
ymin = -2.1
ymax = 2.1
zmin = -1.1
zmax =  p*n*2+1.1
x = np.linspace(xmin, xmax, gs)  # Positions for x
y = np.linspace(ymin, ymax, gs)  # Positions for y
z = np.linspace(zmin, zmax, gs)  # Positions for z
Y, Z = np.meshgrid(y, z, indexing='ij')  # Grid for y/z

# Cell/beads
Rb = 3.5e-6
Rc = 3.5e-5
muo = np.pi*4e-7
muw = 10e-3
chi = 0.17
rhob = 1.5e3
rhoc = 1020
rhow = 1000
g = 9.81

MagConst = (4*np.pi*Rb**3*chi/(3*muo))
ViscConst = 6*np.pi*muw*Rc
m = (4/3)*np.pi*Rb**3*rhob + (4/3)*np.pi*(Rc**3-Rb**3)*rhoc
Vc = (4/3)*np.pi*Rc**3
Vb = (4/3)*np.pi*Rb**3

# Book keeping
BdotGradB = np.zeros([1, 3])
V = np.zeros(3)
tstep = 0.01
t0 = 0
t1 = 1
t = np.arange(t0, t1, tstep)

Nb = int(sys.argv[2])
Vt = g*(rhoc-rhow)*Vc/(6*np.pi*muw*Rc) #terminal velocity
L = 1e-2

# Function to do summation over all segments of wire
def find_B(pos, theta, R, N):
    cross = 0
    for k in range(1, theta.size):
        rs = np.array([R*np.cos(theta[k]-np.pi/N),
```

```
                        R*np.sin(theta[k]-np.pi/N),
                        (p*(theta[k]-np.pi/N))/np.pi])
            r = pos - rs
            dl = np.array([R*(np.cos(theta[k])-np.cos(theta[k-1])),
                        R*(np.sin(theta[k])-np.sin(theta[k-1])),
                        p/N])
            cross += C * np.cross(dl, r) / LA.norm(r)**3
    return cross

# Function to do summation over all segments of wire V2
def find_B_v2(pos, theta, R, N):
    cross = 0
    for k in range(1, theta.size):
        dlCrossR = np.array([R*(pos[2]-(p/(2*N))*(2*k-1))*
                    (np.sin(theta[k])-np.sin(theta[k-1]))-
                    (p/(2*N))*
                    (pos[1]-R*np.sin(theta[k]-(theta[1]-theta[2])/2)),
                    -R*(pos[2]-(p/(2*N))*(2*k-1))*
                    (np.cos(theta[k])-np.cos(theta[k-1]))+
                    (p/(2*N))*(pos[0]-
                        R*np.cos(theta[k]-(theta[1]-theta[2])/2)),
                    -R*pos[0]*(np.sin(theta[k])-
                        np.sin(theta[k-1]))+R*pos[1]*
                        (np.cos(theta[k])-np.cos(theta[k-1]))+
                        2*R**2*np.sin((theta[1]-theta[2])/2)])
        cross += dlCrossR/ math.sqrt((R**2+pos[0]**2+pos[1]**2+
                                (pos[2]-(p/(2*N))*(2*k-1))**2 -
                                2*R*(pos[0]*
                                np.cos(theta[k]-(theta[1]-theta[2])/2) +
                                pos[1]*
                                np.sin(theta[k]-(theta[1]-theta[2])/2)))**3)
    return cross

def Diff_find_Bs():
    posValsX=np.linspace(-0.5,0.5,100)
    posValsY=0
    posValsZ=3

    with open('B_diff.dat','a+') as f:
        f.write("x y z diffBX diffBY diffBZ\n")
        for i in range(size(posValsX)):
            pos = np.array([posValsX[i], posValsY, posValsZ])
            Bx1, By1, Bz1 = find_B(pos,theta,R,N)
            Bx2, By2, Bz2 = find_B_v2(pos,theta,R,N)
            Bxdiff = abs(Bx1 - Bx2)
```

```
            Bydiff = abs(By1 - By2)
            Bzdiff = abs(Bz1 - Bz2)
            f.write("%.8f %.8f %.8f %.8f %.8f %.8f\n" %
                    (posValsX[i], posValsY,
                     posValsZ, Bxdiff, Bydiff, Bzdiff ))

def find_BdotGradB(pos):
    h = np.pi*R/N

    Bx, By, Bz = find_B(pos, theta, R, N)

    Bx_right, By_right, Bz_right = find_B(pos + [0,h,0], theta, R, N)
    Bx_left, By_left, Bz_left = find_B(pos - [0,h,0], theta, R, N)
    Bx_up, By_up, Bz_up = find_B(pos + [0,0,h], theta, R, N)
    Bx_down, By_down, Bz_down = find_B(pos - [0,0,h], theta, R, N)

    bxy = (Bx_right - Bx_left) / 2*h
    byy = (By_right - By_left) / 2*h
    bzy = (Bz_right - Bz_left) / 2*h

    bxz = (Bx_up - Bx_down) / 2*h
    byz = (By_up - By_down) / 2*h
    bzz = (Bz_up - Bz_down) / 2*h

    # X derivatives calculated by divergence and curl of B
    bxx = -byy - bzz
    byx =  bxy
    bzx =  - bxz
    return [Bx*bxx + By*bxy + Bz*bxz, Bx*byx + By*byy + Bz*byz,
            Bx*bzx + By*bzy + Bz*bzz]


def func(X, t):
    xval = 0
    yval = 0
    zval = -1
    return [xval, yval, zval]

def funcmag(X, t):
    pos = np.array([X[0], X[1], X[2]])
    BdotGradB = find_BdotGradB(pos)
    xval = (Nb/Vt)*(Vb*chi/(muw*muo*6*np.pi*Rc))*(1/L)*BdotGradB[0]
    yval = (Nb/Vt)*(Vb*chi/(muw*muo*6*np.pi*Rc))*(1/L)*BdotGradB[1]
    zval = -1 + (Nb/Vt)*(Vb*chi/(muw*muo*6*np.pi*Rc))*(1/L)*BdotGradB[2]
    return [xval, yval, zval]
```

```
def run(X0):
    X = odeint(func, X0, t)
    Xmag = odeint(funcmag,X0,t)
    #print(Xmag[:,2])
    return X, Xmag

def singleTraj():
    X0 = [0, 0.1, 2*p*n+1]
    X, Xmag = run(X0)
    with open('trajX_TEST.dat','a+') as f:
        f.write("x y z\n")
        for i in range(size(t)):
            if X[i,2] < 2*p*n:
                break
            f.write("%.4f %.4f %.4f\n" % (X[i,0], X[i,1], X[i,2]))

    with open('trajXmag_TEST.dat','a+') as f:
        f.write("x y z\n")
        for i in range(size(t)):
            if Xmag[i,2] < 2*p*n:
                break
            f.write("%.8f %.8f %.8f\n" % (Xmag[i,0],
                                          Xmag[i,1], Xmag[i,2]))

def multiTraj():
    for i in tqdm(range(0, 5)):
        X0= [0.2*i,0.2*i, 2*p*n+1]
        Xmag = odeint(funcmag,X0,t)

        with open('trajXmagRT_{0}.dat'.format(i),'a+') as f:
            f.write("x y z\n")
            for i in range(size(t)):
                if Xmag[i,2] < 2*p*n:
                    break
                f.write("%.8f %.8f %.8f\n" % (Xmag[i,0], Xmag[i,1],
                                              Xmag[i,2]))

    for i in tqdm(range(1, 5)):
        X0= [-0.2*i,-0.2*i, 2*p*n+1]
        Xmag = odeint(funcmag,X0,t)

        with open('trajXmagLB_{0}.dat'.format(i),'a+') as f:
            f.write("x y z\n")
```

```
            for i in range(size(t)):
                if Xmag[i,2] < 2*p*n:
                    break
                f.write("%.8f %.8f %.8f\n" % (Xmag[i,0], Xmag[i,1],
                                              Xmag[i,2]))

    for i in tqdm(range(1, 5)):
        X0= [0.2*i,-0.2*i, 2*p*n+1]
        Xmag = odeint(funcmag,X0,t)

        with open('trajXmagRB_{0}.dat'.format(i),'a+') as f:
            f.write("x y z\n")
            for i in range(size(t)):
                if Xmag[i,2] < 2*p*n:
                    break
                f.write("%.8f %.8f %.8f\n" % (Xmag[i,0], Xmag[i,1],
                                              Xmag[i,2]))

    for i in tqdm(range(1, 5)):
        X0= [-0.2*i,0.2*i, 2*p*n+1]
        Xmag = odeint(funcmag,X0,t)

        with open('trajXmagLT_{0}.dat'.format(i),'a+') as f:
            f.write("x y z\n")
            for i in range(size(t)):
                if Xmag[i,2] < 2*p*n:
                    break
                f.write("%.8f %.8f %.8f\n" % (Xmag[i,0], Xmag[i,1],
                                              Xmag[i,2]))

def circTraj():
    for i in tqdm(range(0, 12)):
        thetaval = i*2*np.pi/12
        X0= [np.cos(thetaval), np.sin(thetaval), 2*p*n+1]
        Xmag = odeint(funcmag,X0,t)

        with open('trajXmagCircFar_{0}.dat'.format(i),'a+') as f:
            f.write("x y z\n")
            for i in range(size(t)):
                if Xmag[i,2] < 2*p*n:
                    break
                f.write("%.8f %.8f %.8f\n" % (Xmag[i,0], Xmag[i,1],
                                              Xmag[i,2]))

    for i in tqdm(range(0, 12)):
```

```
        thetaval = i*2*np.pi/12
        X0= [0.5*np.cos(thetaval), 0.5*np.sin(thetaval), 2*p*n+1]
        Xmag = odeint(funcmag,X0,t)

        with open('trajXmagCircClose_{0}.dat'.format(i),'a+') as f:
            f.write("x y z\n")
            for i in range(size(t)):
                if Xmag[i,2] < 2*p*n:
                    break
                f.write("%.8f %.8f %.8f\n" % (Xmag[i,0], Xmag[i,1],
                                              Xmag[i,2]))

    for i in tqdm(range(0, 12)):
        thetaval = i*2*np.pi/12
        X0= [0.25*np.cos(thetaval), 0.25*np.sin(thetaval), 2*p*n+1]
        Xmag = odeint(funcmag,X0,t)

        with open('trajXmagCircVClose_{0}.dat'.format(i),'a+') as f:
            f.write("x y z\n")
            for i in range(size(t)):
                if Xmag[i,2] < 2*p*n:
                    break
                f.write("%.8f %.8f %.8f\n" % (Xmag[i,0], Xmag[i,1],
                                              Xmag[i,2]))

def distTraj():
    for i in tqdm(range(0, 4)):
        X0= [(0.75+(float(i)/10.))*np.cos(pi/4),(0.75+(float(i)/10.))*
             np.sin(pi/4), 2*p*n+1]
        Xmag = odeint(funcmag,X0,t)

        with open('trajXmagDist_{0}.dat'.format(i+12),'a+') as f:
            f.write("x y z\n")
            for i in range(size(t)):
                if Xmag[i,2] < 2*p*n:
                    break
                f.write("%.8f %.8f %.8f\n" % (Xmag[i,0], Xmag[i,1],
                                              Xmag[i,2]))

def multiBead():
    X0 = [0, 0, 2*p*n+1]
    Xmag = odeint(funcmag,X0,t)

    with open('trajXmagMulti_{0}.dat'.format(Nb),'a+') as f:
        f.write("x y z\n")
```

```
        for i in range(size(t)):
            if Xmag[i,2] < 2*p*n:
                break
            f.write("%.1f %.8f %.8f %.8f\n" % (i+1, Xmag[i,0], Xmag[i,1],
                                               Xmag[i,2]))

if __name__ == '__main__':
    for i in range(0, theta.size):
        theta[i] = i*2*np.pi/N

    multiTraj()
    Diff_find_Bs()
    circTraj()
    distTraj()
    singleTraj()
    multiBead()
```

APPENDIX C

Cross Product Reference Sheet

$$\mathbf{e}_x \times \mathbf{e}_y = \mathbf{e}_z, \qquad \mathbf{e}_y \times \mathbf{e}_z = \mathbf{e}_x, \qquad \mathbf{e}_z \times \mathbf{e}_x = \mathbf{e}_y$$

$$\mathbf{e}_x \times \hat{\mathbf{r}}_m = \begin{vmatrix} \mathbf{e}_x & \mathbf{e}_y & \mathbf{e}_z \\ 1 & 0 & 0 \\ \cos\theta_m & \sin\theta_m & 0 \end{vmatrix} = \sin\theta_m \mathbf{e}_z,$$

$$\mathbf{e}_x \times \hat{\theta}_m = \begin{vmatrix} \mathbf{e}_x & \mathbf{e}_y & \mathbf{e}_z \\ 1 & 0 & 0 \\ -\sin\theta_m & \cos\theta_m & 0 \end{vmatrix} = \cos\theta_m \mathbf{e}_z,$$

$$\mathbf{e}_y \times \hat{\mathbf{r}}_m = \begin{vmatrix} \mathbf{e}_x & \mathbf{e}_y & \mathbf{e}_z \\ 0 & 1 & 0 \\ \cos\theta_m & \sin\theta_m & 0 \end{vmatrix} = -\cos\theta_m \mathbf{e}_z,$$

$$\mathbf{e}_y \times \hat{\theta}_m = \begin{vmatrix} \mathbf{e}_x & \mathbf{e}_y & \mathbf{e}_z \\ 0 & 1 & 0 \\ -\sin\theta_m & \cos\theta_m & 0 \end{vmatrix} = \sin\theta_m \mathbf{e}_z,$$

$$\mathbf{e}_z \times \hat{\mathbf{r}}_m = \begin{vmatrix} \mathbf{e}_x & \mathbf{e}_y & \mathbf{e}_z \\ 0 & 0 & 1 \\ \cos\theta_m & \sin\theta_m & 0 \end{vmatrix} = \hat{\theta}_m$$

$$\mathbf{e}_z \times \hat{\theta}_m = \begin{vmatrix} \mathbf{e}_x & \mathbf{e}_y & \mathbf{e}_z \\ 0 & 0 & 1 \\ -\sin\theta_m & \cos\theta_m & 0 \end{vmatrix} = -\hat{\mathbf{r}}_m,$$

$$\hat{\mathbf{r}}_m \times \hat{\theta}_m = \begin{vmatrix} \mathbf{e}_x & \mathbf{e}_y & \mathbf{e}_z \\ \cos\theta_m & \sin\theta_m & 0 \\ -\sin\theta_m & \cos\theta_m & 0 \end{vmatrix} = \mathbf{e}_z$$

APPENDIX D

Human Umbilical Vein Endothelial Cells

The following document is the data sheet for the human umbilical vein endothelial cells. It can be found at www.sciencellonline.com [27].

Human Umbilical Vein Endothelial Cells (HUVEC)
Catalog #8000

Cell Specification
Vascular endothelial cells contribute to the maintenance of vascular homeostasis. Vascular endothelial cells produce and secrete activators and inhibitors of the coagulation and fibrinolysis system. In addition, they mediate the adhesion and aggregation of blood platelets. Endothelial cells also release molecules that regulate cell proliferation and control vessel wall tone. Human umbilical vein endothelial cells (HUVEC) are the most commonly used cell type for the study of endothelial cell processes *in vitro*. HUVEC have a "cobblestone" morphology, show positive staining for vWF/Factor VIII and CD-31, and the ability to take up acetylated low-density lipoprotein [1, 2]. Cells pretreated with IL-1 or TNF-alpha also selectively express E-selectin [3] and VCAM [4].

HUVEC from ScienCell Research Laboratories are isolated from human umbilical veins. HUVEC are cryopreserved at passage one and delivered frozen. Each vial contains >5 x 10^5 cells in 1 ml volume. HUVEC are characterized by immunofluorescence with antibodies specific to vWF/Factor VIII and CD31. HUVEC are negative for HIV-1, HBV, HCV, mycoplasma, bacteria, yeast and fungi. HUVEC are guaranteed to further expand for 15 population doublings under the conditions provided by ScienCell Research Laboratories.

Recommended Medium
It is recommended to use endothelial cell medium (ECM, Cat. #1001) for the culturing of HUVEC *in vitro*.

Product Use
HUVEC are for research use only. They are not approved for human or animal use, or for application in *in vitro* diagnostic procedures.

Storage
Upon receiving, directly and immediately transfer the cells from dry ice to liquid nitrogen and keep the cells in liquid nitrogen until they are needed for experiments.

Shipping
Dry ice.

References
[1] Morgan DML. (1996) "Isolation and culture of human umbilical vein endothelial cells." In Jones GE, *Human Cell Culture Protocols* (pp 104-109) Totowa: Humana Press.
[2] Newman PJ, Berndt MC, Gorski J, White GC, Lyman S, Paddock C, Muller WA. (1990) "PECAM-1 (CD31) cloning and relation to adhesion molecules of the immunoglobulin gene superfamily." *Science*. 247:1219-1222.
[3] Bevilaqua MP, Stengelin S, Gimbrone MA, Seed B. (1989) "Endothelial leukocyte adhesion molecule 1: an inducible receptor for neutrophils related to complement regulatory proteins and lectins." *Science* 243:1160-1165.
[4] Osborn L, Hession C, Tizard R, Vassallo C, Luhowskyj S, Chi-Rosso G, Lobb R. (1989) "Direct cloning of vascular cell adhesion molecule 1, a cytokine induced endothelial protein that binds to lymphocytes." *Cell* 59:1203-1211.

Instructions for culturing cells

Caution: Cryopreserved cells are very delicate. Thaw the vial in a 37°C water bath and return the cells to culture as quickly as possible with minimal handling!

Initiating the culture:

1. Prepare a fibronectin-coated culture vessel (2 μg/cm^2, T-75 flask is recommended). Add 5 ml of sterile Dulbecco's phosphate buffered saline, Ca^{++}- and Mg^{++}-free (Cat. #0303) to a T-75 flask and then add 150 μl of fibronectin stock solution (Cat. #8248). Leave the vessel in a 37°C incubator overnight.
2. Prepare complete medium. Decontaminate the external surfaces of medium bottle and medium supplement tubes with 70% ethanol and transfer them to a sterile field. Aseptically transfer supplement to the basal medium with a pipette. Rinse the supplement tube with medium to recover the entire volume.
3. Aspirate fibronectin solution and add 15 ml of complete medium to the culture vessel. The fibronectin solution can be used twice. Leave the vessel in the sterile field and proceed to thaw the cryopreserved cells.
4. Place the frozen vial in a 37°C water bath. Hold and rotate the vial gently until the contents completely thaw. Promptly remove the vial from the water bath, wipe it down with 70% ethanol, and transfer it to the sterile field.
5. Carefully remove the cap without touching the interior threads. Gently resuspend and dispense the contents of the vial into the equilibrated, fibronectin-coated culture vessel. A seeding density of 5,000-7,000 cells/cm^2 is recommended.

   Note: Dilution and centrifugation of cells after thawing are not recommended since these actions are more harmful to the cells than the effect of residual DMSO in the culture. It is also important that cells are plated in fibronectin-coated culture vessels to promote cell attachment.
6. Replace the cap or lid of the culture vessel and gently rock the vessel to distribute the cells evenly. Loosen cap, if necessary, to allow gas exchange.
7. Return the culture vessel to the incubator.
8. For best results, do not disturb the culture for at least 16 hours after the culture has been initiated. Refresh culture medium the next day to remove residual DMSO and unattached cells, then every other day thereafter.

Maintaining the culture:

1. Refresh supplemented culture medium the next morning after establishing a culture from cryopreserved cells.
2. Change the medium every three days thereafter, until the culture is approximately 70% confluent.

3. Once the culture reaches 70% confluency, change medium every other day until the culture is approximately 90% confluent.

Subculturing:

1. Subculture when the culture reaches 90-95% confluency.
2. Prepare fibronectin-coated culture vessels (2 μg/cm^2) one day before subculture.
3. Warm complete medium, trypsin/EDTA solution (T/E, Cat. #0103), T/E neutralization solution (TNS, Cat. #0113), and DPBS (Ca^{++}- and Mg^{++}-free, Cat. #0303) to **room temperature**. We do not recommend warming reagents and medium in a 37^{o}C water bath prior to use.
4. Rinse the cells with DPBS.
5. Add 10 ml of DPBS and then 1 ml of T/E solution into flask (in the case of a T-75 flask). Gently rock the flask to ensure complete coverage of cells by T/E solution. Incubate the flask in a 37^{o}C incubator for 1 to 2 minutes or until cells completely round up. Use a microscope to monitor the change in cell morphology.
6. During incubation, prepare a 50 ml conical centrifuge tube with 5 ml of fetal bovine serum (FBS, Cat. #0500).
7. Transfer T/E solution from the flask to the 50 ml centrifuge tube (a small percent of cells may detach) and continue to incubate the flask at 37^{o}C for another 1 to 2 minutes (no solution in the flask at this moment).
8. At the end of incubation, gently tap the side of the flask to dislodge cells from the surface. Check under a microscope to make sure that all cells detach.
9. Add 5 ml of TNS solution to the flask and transfer detached cells to the 50 ml centrifuge tube. Rinse the flask with another 5 ml of TNS to collect the residual cells.
10. Examine the flask under a microscope for a successful cell harvest by looking at the number of cells being left behind; there should be less than 5%.

    Note: Use ScienCell T/E solution that is optimized to minimize cell damages due to over trypsinization.
11. Centrifuge the 50 ml centrifuge tube at 1000 rpm for 5 minutes. Resuspend cells in culture medium.
12. Count and plate cells in a new fibronectin-coated culture vessel with the recommended cell density.
13. Subculture the cells when they are over 90% confluent.

Caution: Handling human derived products is potentially biohazardous. Although each cell strain tests negative for HIV, HBV and HCV DNA, diagnostic tests are not necessarily 100% accurate, therefore, proper precautions must be taken to avoid inadvertent exposure. Always wear gloves and safety glasses when working with these materials. Never mouth pipette. We recommend following the universal procedures for handling products of human origin as the minimum precaution against contamination [1].

[1] Grizzle WE, Polt S. (1988) "Guidelines to avoid personal contamination by infective agents in research laboratories that use human tissues." *J Tissue Culture Methods*. 11: 191-9.

APPENDIX E

Anti-Biotin MACSiBead^{TM} Particles

The following document is the data sheet for the MACSiBead magnetic particles. It can be found at www.miltenyibiotec.com [25].

Miltenyi Biotec

Anti-Biotin MACSiBead™ Particles

Order no. 130-091-147

Contents

1. Description

Components	2.5 mL Anti-Biotin MACSiBead™ Particles: MACSiBead Particles (appr. 3.5 µm diameter) conjugated to monoclonal anti-biotin antibodies (isotype: mouse IgG1); anti-biotin antibodies do not bind to free biotin.
Capacity	For separation of 5×10^8 total cells.
Product format	Anti-Biotin MACSiBead Particles are supplied in buffer containing 0.05% sodium azide.
Storage	Store protected from light at 2 – 8 °C. Do not freeze. The expiration date is indicated on the vial label.

1.1 Principle of a separation using Anti-Biotin MACSiBead™ Particles

First, the cells are labeled with biotinylated primary antibodies. In a second step, the biotin-labeled cells are magnetically labeled with Anti-Biotin MACSiBead™ Particles. Subsequently, the cell suspension is placed in the magnetic field of a MACSiMAG™ Separator. The bead-labeled cells migrate towards the magnet and adhere to the wall of the tube. The non-labeled cells in the supernatant are pipetted off and collected as the non-labeled target cell fraction.

1.2 Background information

Anti-Biotin MACSiBead Particles have been developed for depletion of non-target cells using (cocktails of) biotinylated antibodies. Depletion of non-target cells using Anti-Biotin MACSiBead Particles can be combined with positive selection using MACS® MicroBeads.

1.3 Applications

- Depletion of non-target cells from peripheral blood mononuclear cells (PBMCs) or lymphoid tissue.
- Two-step magnetic cell separation by depletion with Anti-Biotin MACSiBead Particles followed by positive selection with MACS MicroBeads.

1.4 Reagent and instrument requirements

- Buffer: Prepare a solution containing phosphate-buffered saline (PBS), pH 7.2, 0.5% bovine serum albumin (BSA), and 2 mM EDTA by diluting MACS BSA Stock Solution (# 130-091-376) 1:20 with autoMACS™ Rinsing Solution (# 130-091-222). Keep buffer cold (2–8 °C).

  ▲ **Note:** EDTA can be replaced by other supplements such as anticoagulant citrate dextrose formula-A (ACD-A) or citrate phosphate dextrose (CPD). BSA can be replaced by other proteins such as human serum albumin, human serum, or fetal bovine serum (FBS). Buffers or media containing Ca^{2+} or Mg^{2+} are not recommended for use.
- 5 mL tubes for up to 1×10^8 total cells or 15 mL tubes for $>1\times10^8$ total cells.
- MACSmix™ Tube Rotator (# 130-090-753) for incubation of cells with Anti-Biotin MACSiBead Particles.
- MACSiMAG Separator for removal of cells labeled with Anti-Biotin MACSiBead Particles.

  ▲ **Note:** Do **not** use MACSiBead Particles with MACS Columns and MiniMACS™, MidiMACS™, OctoMACS™, QuadroMACS, VarioMACS™, SuperMACS™ II, or autoMACS™ Separators.
- (Optional) Fluorochrome-conjugated antibodies, for example Anti-Biotin-FITC (# 130-090-875), Anti-Biotin-PE (# 130-090-756) or Anti-Biotin-APC (# 130-090-856).

2. Protocol

2.1 Sample preparation

When working with anticoagulated peripheral blood or buffy coat, peripheral blood mononuclear cells (PBMCs) should be isolated by density gradient centrifugation, for example, using Ficoll-Paque™.

▲ **Note:** To remove platelets after density gradient separation, resuspend cell pellet in buffer and centrifuge at 200×g for 10–15 minutes at 20 °C. Carefully aspirate supernatant. Repeat washing step.

When working with tissues or lysed blood, prepare a single-cell suspension using standard methods.

For details see the protocols section at www.miltenyibiotec.com/protocols.

▲ Dead cells may bind non-specifically to MACS MicroBeads. To remove dead cells, we recommend using density gradient centrifugation or the Dead Cell Removal Kit (# 130-090-101).

140-000-881.05

Miltenyi Biotec GmbH
Friedrich-Ebert-Straße 68, 51429 Bergisch Gladbach, Germany
Phone +49 2204 8306-0, Fax +49 2204 85197
macs@miltenyibiotec.de
www.miltenyibiotec.com

Miltenyi Biotec Inc.
2303 Lindbergh Street, Auburn, CA 95602, USA
Phone 800 FOR MACS, +1 530 888 8871, Fax +1 530 888 8925
macs@miltenyibiotec.com

Order no. 130-091-147

2.2 Magnetic labeling

▲ Resuspend Anti-Biotin MACSiBead Particles thoroughly before use, to obtain a homogenous dispersion of MACSiBead Particles in solution.

▲ When working with up to 1×10^8 total cells, optimal magnetic labeling is achieved using a 5 mL tube (up to 2 mL total volume for magnetic labeling). When working with higher cell numbers, use a 15 mL tube (>2 mL total volume for magnetic labeling).

1. Determine cell number.
2. Centrifuge cell suspension at 300×g for 10 minutes. Aspirate supernatant completely.
3. Resuspend cell pellet and label cells with the primary biotinylated antibody at a final concentration of 1–5 µg/mL or at the titer recommended by the manufacturer.
   ▲ **Note:** It is recommended to label up to 5×10^7 cells in a total volume of 500 µL. When working with higher cell numbers, scale up all reagent and buffer volumes.
   ▲ **Note:** The biotinylated antibody should be used at its optimal titer, i.e. with optimal labeling intensity and no background labeling.
4. Mix well and incubate for 10 minutes in the refrigerator (2–8 °C).
5. Wash cells by adding 5 mL of buffer per 5×10^7 cells and centrifuge at 300×g for 10 minutes. Aspirate supernatant completely.
6. Repeat washing step 5 and aspirate supernatant completely.
   (Optional) For immunofluorescent staining take an aliquot of the starting material before labeling with Anti-Biotin MACSiBead Particles.
   ▲ **Note:** The aliquot can be stained with fluorochrome-conjugated anti-biotin antibodies (for details, please refer to the Anti-Biotin-FITC, -PE or -APC data sheets.)
7. For up to 5×10^7 cells, resuspend cells in 750 µL of buffer and add 250 µL of Anti-Biotin MACSiBead Particles.
   ▲ **Note:** When working with higher cell numbers, scale up all reagent and buffer volumes accordingly (e.g for 1×10^8 total cells use twice the volume of buffer and Anti-Biotin MACSiBead Particles). When working with fewer than 5×10^7 total cells, use the same volumes as for 5×10^7 total cells.
8. Mix well and incubate for 15 minutes at 2–8 °C using the MACSmix™ Tube Rotator (medium speed/8 rpm).
9. Proceed to magnetic separation (2.3).

2.2 Magnetic separation

1. Place the tube with cells labeled with Anti-Biotin MACSiBead Particles in the magnetic field of a MACSiMAG Separator. Use tube rack to insert tubes from 1.5 mL to 5 mL in size. For more details, see MACSiMAG Separator data sheet.
   ▲ Note: Carefully resuspend cells. To avoid unintended detachment of MACSiBead Particles from magnetically labeled cells, do not vortex.
2. Allow the MACSiBead-labeled cells to adhere to the wall of the tube:

0.5 mL, 1.5 mL, 2 mL, or 5 mL tubes:	2 minutes
15 mL or 50 mL tubes:	4 minutes

3. Retaining the tube in the MACSiMAG Separator, carefully pipette supernatant containing the non-labeled target cells into a new tube.
4. (Optional) To remove residual MACSiBead Particles, replace tube with non-labeled target cells in the MACSiMAG Separator and repeat steps 2 and 3.
   ▲ **Note:** The non-labeled target-cell fraction or an aliquot thereof can be stained with fluorochrome-conjugated Anti-Biotin antibodies (for details, please refer to the Anti-Biotin-FITC, -PE, or -APC data sheets).

3. Example of a T cell depletion using the Anti-Biotin MACSiBead™ Particles

Depletion of T cells from human PBMCs using CD3-Biotin and Anti-Biotin MACSiBead Particles. Cells are fluorescently stained with CD3-APC. The magnetically labeled cells were stained with CellTracker™ CMFDA (Molecular Probes) for flow cytometric discrimination of viable cells from dead cells and Anti-Biotin MACSiBead Particles.

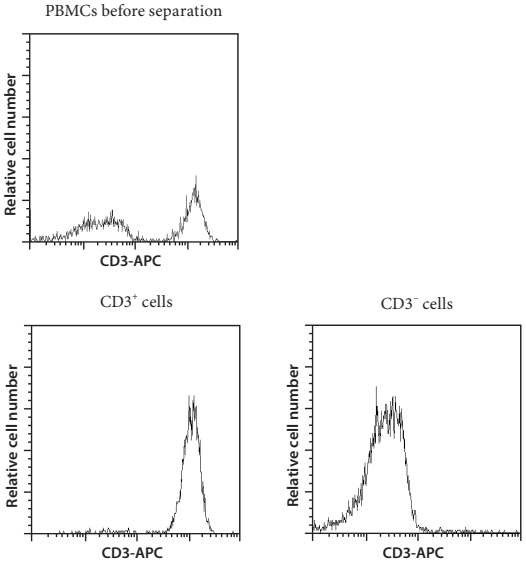

All protocols and data sheets are available at www.miltenyibiotec.com.

Warnings

Reagents contain sodium azide. Under acidic conditions sodium azide yields hydrazoic acid, which is extremely toxic. Azide compounds should be diluted with running water before discarding. These precautions are recommended to avoid deposits in plumbing where explosive conditions may develop.

Warranty

The products sold hereunder are warranted only to be free from defects in workmanship and material at the time of delivery to the customer. Miltenyi Biotec GmbH makes no warranty or representation, either expressed or implied, with respect to the fitness of a product for a particular purpose. There are no warranties, expressed or implied, which extend beyond the technical specifications of the products. Miltenyi Biotec GmbH's liability is limited to either replacement of the products or refund of the purchase price. Miltenyi Biotec GmbH is not liable for any property damage, personal injury or economic loss caused by the product.

140-000-881.05